SUSTAINED PRESENTATION OF THERAPEUTIC FACTORS

By

CHRISTOPHER J LOWE

A dissertation submitted to the

School of Graduate Studies

Rutgers, The State University of New Jersey

In partial fulfillment of the requirements

For the degree of

Doctor of Philosophy

Graduate Program in Biomedical Engineering

Written under the direction of

David I. Shreiber

And approved by

____

____

____

____

____

New Brunswick, New Jersey

October 2018

ABSTRACT OF THE DISSERTATION

By CHRISTOPHER J LOWE

Dissertation Director: David I. Shreiber

The continued development of complex protein therapeutics as life saving medicines has greatly improved outcomes and quality of life for countless patients. Unfortunately, these large complex proteins are not as stable as traditional small molecule drugs and are most commonly administered intravenously, placing burdens on patients who depend on regular dosing. To alleviate these burdens, alternative methods of sustaining therapeutically relevant doses of medicines at sites of injury or disease must be investigated. This dissertation proposes and explores novel methods of sustaining the presentation of therapeutic factors and targeting them to injured and diseased tissues by using native free radicals as a homing signal. Elevated concentrations of free radicals are a characteristic comorbidity of many different injury and disease conditions. In polymer chemistry, free radicals are frequently used to initiate crosslinking and polymerization reactions. We hypothesize that the free radicals characteristic of injured and diseased tissues are capable of inducing crosslinking of acrylate groups. By using acrylated polymers, such as polyethylene glycol diacrylate (PEGDA), coupled to therapeutic factors, this allows for specific targeting and immobilization of these therapeutic factors to injured or diseased tissues with elevated concentrations of free radicals. Further, the interaction of free radicals may reduce or sequester free radicals, limiting their ability to further damage the tissue. Reactive oxygen species (ROS) initiated crosslinking of acrylated PEGs, which enabled the immobilization of a fluorescent payload within tissue mimics. The crosslinking efficiency and immobilization potential varied with the polymer chain length, which suggests that a tunable platform can be achieved. Thiol and alkene functionalized PEGs also demonstrated good crosslinking potential with native free radicals and offer an additional avenue of platform customization. Additionally, the reaction of these functionalized PEGs with free radicals protected cells from the damaging effects of oxidative stress in vitro. Together these results provide promising proof of concept for using free radicals as a means of specifically targeting and sustaining drugs to injured or diseased tissues. Overall the work described in this dissertation has the potential to serve as the building block for improved strategies for administering complex therapeutics to patients in need.

DEDICATION

“Learning is the most important thing we do.”

ACKNOWLEDGEMENTS

These last six years have been a challenging and rewarding experience that has allowed me to grow as a research scientist and engineer. While a PhD is an immensely personal challenge it is also an incredible collaborative endeavor and I have many people to thank for their guidance and support throughout the process.

Thank you to my adviser, Dr. David I. Shreiber for all of your guidance and training during my time in the laboratory. It was roundabout how I eventually ended up joining Dr. Shreiber's laboratory early in my PhD training, but I could not have asked for a more perfect match for an adviser. Thank you for all your guidance and support as I navigated my projects in the lab and adapted to new endeavors outside of the lab.

Thank you to members of my thesis committee, Dr. Martin Yarmush, Dr. Joseph Freeman, and Dr. Janet Alder. I was grateful for your feedback and support provided from you all as a committee, but I am also so very grateful for my experiences with each of you outside of my committee as well: Dr. Yarmush through the Biotechnology Training Program and the GAANN Fellowship, Dr. Freeman through a first-year rotation and within the BME community, and Dr. Alder through the iJOBS program. Each of these experiences helped my grow tremendously over the past six years and I would not be in the same position I am now without you all.

Thank you to all of the organizations which provided support to me during my time at Rutgers: the New Jersey Commission on Brain Injury Research (NJCBIR), the Department of Education's Graduate Assistance in Areas of National Need (GAANN) Fellowship, the Rutgers Biotechnology Training Program, the National Institutes of Health, the Rutgers Interdisciplinary Job Opportunities for Biomedical Scientists (iJOBS) program, and the Rutgers REU in Cellular Bioengineering.

Thank you to members of the Shreiber Laboratory, both past and present: Kathryn Drzewiecki, Sagar Singh, Madison Godesky, Joe Sherba, Yoliem Miranda Alarcon, Emily DiMartini, Timo Roehrs, David Sillitti, Han Chen, Mihir Moghe and many more. We were all in it together on a daily basis and I am so glad to have had the chance to work with you and get to know you all both in the lab and out. No other workplace will be as fun or as unique as the one we all shared together.

Thank you to former undergraduate students I had the pleasure of mentoring: Ian Reucroft, Matthew Grota, Keana Mirmajlesi, Trevor Alston, Emily DiMartini, and Victor Suarez. I thoroughly enjoyed the time I was able to spend both teaching and learning from you all through my entire time at Rutgers. I was fortunate to have had the chance to work with so many talented, motivated, and interesting young scientists and I am excited to see what lays ahead for you in all of your careers.

Thank you to those who collaborated and contributed to the success of this thesis research. Specifically, I would like to acknowledge Dr. Adam Gormley, Shashank Kosuri, and Rahul Upadhya for being so accommodating and helpful with the GPC instrument. I learned much from working with the three of you and it added a great deal to the project. I would also like to thank Dr. Nagarajan Murali and Dr. Sheo Kim for their time and expertise in utilizing the NMR Research Facility.

Thank you to the BME support staff: Larry Stromberg, Robin Yarborough, Mary Ellen Presa, and Mary Creteau, for all of your time and effort on my behalf. You were all always willing to take the time to address our needs as students and help things run smoothly so our focus could always be on the science and our own professional development. The incredible BME community would not be the same without all of you there to help build and reinforce it.

Thank you to everyone from the larger BME community over the past six years. The strong sense of community that was present when I visited Rutgers as a prospective student was one of the selling pieces to me when I made the decision to come to Rutgers. Though the faces were constantly changing and the names are too numerous list here, the sense of family and camaraderie was ever present within the building during my time in the program. It was energizing, supportive, and transformative for me and I was glad to experience and contribute that as a graduate student at Rutgers. Thank you also to my 2011 REU mentor Dr. Aaron Carlson, now a BME alumni. If it had not been for the overwhelmingly positive experience you help create for me that summer, I would not have come to Rutgers for my PhD.

Lastly and most importantly, thank you to my family. Without the constant support and encouragement from my parents, Michael and Susan, and my brother, Shawn, over the past twenty-nine years I would never have been able to be part of an engineering PhD program in the first place, and I certainly would not have been able to make it through the program without their continued support. Words cannot express have truly thankful and grateful I am to have had the three of you in my corner for all of my life and to instill values of hard work, passion, tenacity, and class into me. Words similarly fall short when it comes to thanking my beautiful wife Patricia for all of her patience, support, and understanding over the last six years as I made my way into my PhD and finally out the other side. Lots of life has happened to us in these last six years, an engagement, a wedding, and welcoming two amazing little boys into this world, our sons Dustin and Derek. Patricia, you have constantly amazed me with your capacity for love and understanding as we try our best to do what’s right for our young family while I was still in school. I never would have been able to do this without you. I am so grateful to have you in my life and I love you more than you can know.

TABLE OF CONTENTS

TABLE OF FIGURES

TABLE OF TABLES

CHAPTER 1. INTRODUCTION

1.1 DRUG DELIVERY

The continued evolution of pharmaceutical products and the advent of new biotechnology therapies has had profound effects on the health and well-being of patients. Historically, the pharmaceutical industry has been dominated by small molecule drugs. Small molecule drugs are usually less than 900 Daltons in size, are produced through well-defined chemical synthesis, and are very stable. Because of their high stability, these drugs can often be formulated for oral administration, as they won't be damaged or inactivated by harsh pH conditions present in the digestive tract. Drugs are most frequently administered through regular doses to maintain concentrations of drug within the body that are high enough to have the desired effects. Regular dosing for oral drugs is straightforward and can be done by patients unobtrusively in the home or as they go about their daily lives. Increasingly over the last two decades, biologic drugs have grown their share of the pharmaceutical landscape, and that is expected to grow further in the years to come. Biologics are most commonly large, complex proteins such as antibodies or growth factors. While biologic medicines have greatly improved outcomes and quality of life for patients suffering from many debilitating diseases, biologics are much less stable than small molecule drugs and cannot be delivered orally. Because biologics cannot withstand the harsh pH changes encountered during oral administration, most must be delivered intravenously either in a clinical setting or through trained professionals in the home. Both options place an enormous burden on patients to receive regular doses of medicine. To alleviate this burden, new strategies of sustaining therapeutically relevant doses of medicine at sites of injury and disease are necessary.

Alternative means of delivering and dosing of drugs is not a new problem. Even prior to the rise of biologics, there was great interest in achieving prolonged, localized concentrations of drug for certain conditions. For these applications, drug eluting biomaterials, including polymer coatings or hydrogels that are impregnated with drug, have often been explored. Over time, drug is released, either by diffusing out of the biomaterial or as the biomaterial itself degrades. Unfortunately, while the drug is slowly released over time, once released it is still subject to rapid clearance away from the local injury site. Additionally, the implanted biomaterials can elicit a foreign body response and nonuniform degradation can lead to unintentional overdosing. Further not all drugs are compatible with the chemistries required to incorporate drugs into these drug eluting biomaterials.

1.2 TARGETED DRUG DELIVERY

Another avenue for achieving localized impact of drugs, is through targeted drug delivery. Targeted drug delivery offers the promise for the selective and precise delivery of drug payloads directly to the cells and tissues that require the therapeutic, which can minimize required dosages and off-target side effects.[1] Successful targeted drug delivery requires a balance of specificity and sensitivity. Various types of drug-carrying nanoparticles have been developed to carry a therapeutic agent to the target tissue following systemic delivery.[2] Most often, target-specific ligands are coupled to the nanoparticle surface to selectively bind to a single cell surface receptor.[3-5] In cancer treatment, receptors overexpressed on the tumor cell's surface are identified as substrates for ligand-receptor interactions.[2-4, 6] However, because of the heterogeneity of different types of cancers, this approach requires the discovery of ligands that are unique to cell surface receptors on different types of tumors.[1-2, 4, 6-7] As such, new targets and ligands must be identified for any new application, which is both non-trivial and costly.[5] Further, tumors do not evenly express surface cell receptors throughout the tumor mass, and the expressed receptors continuously change.[2, 6] The heterogeneity within tumors and between tumor types limits the therapeutic capabilities of a ligand-based targeting approach. Additionally, receptors that are overexpressed in tumor cells are also expressed to a lesser degree in healthy cells, which can lead to off-target dumping.[1, 6]

1.3 SUSTAINED PRESENTATION OF THERAPEUTIC FACTORS

Clearance of drug remains an issue when using soluble factors. Covalently tethering the drug to a matrix or polymer backbone has been demonstrated to sustain and even enhance the effects of the coupled factor over a prolonged period. This has been demonstrated in the literature with factors such as epidermal growth factor (EGF), insulin, and brain derived neurotrophic factor (BDNF), all complex biologic proteins.[8-11] Further the covalent attachment prevents the drug from diffusing away from an injury site, resisting clearance in vivo. This has been demonstrated in our own laboratory by immobilizing peptides to type-I collagen hydrogels.[12-16] A prime example of the improved effectiveness of covalently coupled factors over soluble factors is previous work completed with nerve guidance conduits. Two peptide factors were identified which can accelerate and improve healing of transected peripheral nerves. Solubly, these factors were only effective in repairing gaps in the mouse femoral nerve that were 2mm or less. When these peptides were covalently immobilized to collagen, they were effective in repairing 5mm femoral nerve gaps.[12] These results support that there may be great opportunity to enhance the effectiveness of therapeutic factors through covalent coupling to sustain their presentation at an injury site. This work investigates new ways of delivering and sustaining drugs and other therapeutic factors locally to tissues where they are needed most.

1.4 THESIS OVERVIEW

This thesis research seeks to combine aspects of sustained presentation and targeted delivery to a new drug delivery platform that targets free radicals naturally present in injured and diseased tissues. This idea arose following results obtained from our work described in Chapter 2, aimed at developing a peptide grafted collagen that could improve regeneration following traumatic brain injury. While the grafted peptides demonstrated positive results, issues with collagen forced us to abandon collagen as a polymer backbone. Transitioning away from collagen also meant coming up with a new way to localize and immobilize our grafted therapeutics, as we would no longer be able to take advantage of collagen self-assembly. Another material in our laboratory, collagen methacrylamide, leverages free radical induced crosslinking of methacrylate groups to modulate the mechanical properties of collagen. A primary characteristic of secondary injury following TBI is increased production of free radicals. Our hypothesis was that free radicals that are naturally localized to the site of TBI could similarly induce crosslinking of functionalized polymers, thereby localizing these polymers and a coupled therapeutic to the site of TBI. Proof of concept investigating this hypothesis using acrylated polyethylene glycol is described in Chapter 3. As it turns out, elevated concentrations of free radicals are characteristic of a great number of different diseases and tissue injuries. Following positive results with acrylated PEGs, investigation of alternatively functionalized PEGs was performed and is described in Chapter 4. The addition of these other functional groups expand the range of over which the proposed platform can be tailored to, particularly for different drugs or conditions. Together the results described in this dissertation represent proof of concept for our free radical mediated crosslinking and immobilization platform. It is our hope that these results can be expanded and eventually applied to help improve outcomes and quality of life for patients suffering from countless diseases and injuries.

CHAPTER 2. IMMOBILIZED BDNF FRAGMENT PEPTIDE-GRAFTED HYDROGELS TO PROMOTE NEURAL SURVIVAL & REGENERATION

2.1 INTRODUCTION

TBI is a prominent medical concern in New Jersey, the United States, and worldwide. An estimated 175,000 new cases of TBI occur each year in New Jersey alone and as many as 1.7 million new cases occur each year across the United States.[17] The effects of TBI vary greatly depending on the severity and extent of the injury and the specific part of the brain that is injured, but those affected with TBI often face severe disability and reduced quality of life. The central nervous system has limited capacity to self-repair, and currently there are no fully restorative treatments for TBI. The most prevalent causes of TBI include vehicle crashes, falls, violence and sports related injuries.[18-19] These injuries are estimated to incur $60 billion annually in the United States in direct medical costs and indirect costs due to lost productivity.[20] TBI is most prevalent among young adult males who will face the burden of extended disability for the remainder of their life, further reducing their quality of life and exacerbating the economic cost.

Physiologically, TBI encompasses damage to the brain by a variety of means, most often by severe contusion, which can cause damage to neurons and supporting cells in the brain. This initial primary injury is followed by an inflammatory secondary injury cascade that results in the formation of a glial scar. As part of this inflammatory response, neurons in the injured area undergo widespread depolarization and levels of neurotransmitters spike typically causing glutamate induced excitotoxicity. Levels of free radicals are substantially upregulated, indiscriminately damaging cell membranes, proteins, and nucleic acids. Further, the presence of free radicals perpetuates the formation of more free radicals. The prolonged inflammatory response also leads to the formation of a glial scar comprised of microglia, reactive astrocytes, and basal membrane. The glial scar not only poses a physical barrier to regeneration, but cells in this environment secrete a variety of inhibitory factors perpetuating a hostile chemical environment at the site of injury.

Current clinical treatments are limited in both scope and efficacy. Overall no fully restorative treatment for TBI currently exists to reverse the damage done by the initial primary insult. Clinical treatments are currently focused on preserving remaining function and limiting secondary injury. In the immediate aftermath of TBI, the patient must be stabilized, and clinicians often must intervene to correct increased intracranial pressure, hypotension, and hypoxia. These symptoms are treated with medication and in severe instances through surgical intervention, but do not address the damage caused by primary injury.

Neurotrophic factors have long been implicated in the development, maintenance, and survival of the nervous system[21] and promote synaptic function.[22] Brain-derived neurotrophic factor (BDNF) in particular has been identified for its potential in TBI applications.[23-24] BDNF modulates neuronal survival through the activation of the tropomyosin-related kinase-B (TrkB) receptor.[22, 25] In cases where BDNF signaling is specifically blocked over other neurotrophic factors, the survival of cortical neurons is significantly reduced.[26] The presence of BDNF has been demonstrated as neuroprotective in models of brain injury.[27] For example, Vutskits et al. showed that an excess of BDNF was sufficient to rescue neurons from cell death in models where polysialic acid neural cell adhesion molecule was inhibited.[25] Ma et. al showed that increasing the level of BDNF at the site of TBI in a rat model significantly improved synaptic function and promoted functional motor recovery.[28] In a separate model, Willson et al. demonstrated that injections of BDNF induced the reinnervation of the transected olivocerebellar projection in the rat brain.[29] While the introduction of BDNF can improve the survival of neurons after TBI, there are significant issues with the delivery of BDNF to the brain and the injury site. Soluble BDNF has high clearance in vivo and is unable to cross the blood-brain barrier at a therapeutically relevant rate. Biomaterial drug delivery systems are being investigated to circumvent these issues but are currently limited by non-uniform distribution profiles. Some novel approaches for delivery of BDNF to sites of TBI, include the approach reported by Ma et. al. who transplanted NSCs which were genetically modified to overexpress BDNF into the injury site in a rat model of TBI.[28] The survival and localization of transplanted cells was poor, however the therapy did increase levels of BNDF at the injury site, and animals who received the modified NSCs showed significantly improved motor function. In a separate approach, Horne et. al. examined the effect of immobilizing BDNF to electrospun polymer scaffolds for applications in spinal cord repair. While the choice of materials and the desired application do not translate directly to TBI, they demonstrated that the immobilized BDNF promoted higher levels of viability, expression of neuronal markers, and differentiation in cultures of NSCs as compared to soluble BDNF introduced through the culture media. These results demonstrate that immobilized BDNF retains its ability to modulate neural cell behavior suggest that delivery via immobilization offers enhanced potency.[8] A potential alternative to BDNF was recently proposed by Cardenas-Aguayo et. al. who reported the development of tetrapeptides which mimic the neurotrophic activity of BDNF. These peptides were shown to be non-cytotoxic to neurons, to induce the expression of neuronal markers including MAP-2, neurofilament-M, and β-III tubulin, and to induce the activation of the TrkB receptor in in vitro cultures of mouse hippocampal neurons, all consistent with the activity of native BDNF.[22] In addition, the presence of the soluble peptide mimics upregulated the production of endogenous BDNF by the primary neurons in culture.[22] Previous work in our laboratory has increased the efficacy of peptide factors through immobilization to type-I collagen hydrogels.[12-15] Collagen hydrogels are an attractive option for treatment of TBI because of their ability to gel in situ at physiological temperature and pH, forming to the size and shape of the injured area it is injected to, allowing for significantly less invasive surgical implantations.[30] In addition, collagen hydrogels adeptly mimic the soft tissue mechanical properties of the surrounding brain tissue, have tunable porosities which promote cell infiltration[31], and can be easily modified to incorporate factors from the natural extracellular matrix such as fibronectin, laminin, and other cell-adhesive peptide sequences.[32] Collagen based hydrogels have been extensively characterized for neural tissue engineering applications.[31, 33-34] Based on the collective results of these studies, we propose to covalently graft these BDNF peptide mimics to type-I collagen hydrogels to facilitate sustained presentation of the BDNF peptide mimics.

2.2 MATERIALS AND METHODS

2.2.2 Peptide Grafting to Collagen and Collagen Hydrogel Formation

IKRG Peptides were synthesized by GenScript in Piscataway, NJ. The IKRG peptides were covalently coupled to type-I collagen according to protocols previously reported by our laboratory. Briefly, type-I bovine collagen (Elastin Products Company) was reconstituted in 0.02N acetic acid at 3mg/mL. The IKRG peptide is incubated in MES buffer with 1-ethyl-3-(dimethylaminopropyl) carbodiimide (EDC) to activate the C-terminus of the peptide. When this solution is added to the collagen suspension, the activated peptide covalently binds to the amine group on lysine residues in the collagen backbone, resulting in a suspension of peptide grafted collagen. The grafted collagen is then dialyzed to remove all ungrafted peptide and crosslinker from the collagen suspension, lyophilized, and resuspended at the desired concentration.

Native collagen or peptide grafted collagen hydrogels were prepared according to the following recipe for 1ml: 20µL HEPES, 130µL 0.15N NaOH, 100µL 10x MEM, 53µL Medium 199 (Life Technologies), 10µL L-glutamine, 10µL penicillin/streptomycin, and 677µL 3.0mg/mL collagen solution. The final concentration of collagen in the hydrogel suspension was 2.0mg/mL. 300µL of hydrogel suspension was used for each well in a 24 well plate and 150 µL of hydrogel suspension was used in 48 well plates. Plates were incubated at 37°C for 1 hour prior to seeding cells to allow self-assembly of collagen hydrogels.

2.2.3 CGN Outgrowth on Peptide Grafted Hydrogels

Cerebellar granule neurons (CGNs) were isolated from day 6 neonatal rat pups. Cells were seeded directly on top of collagen hydrogel conditions at 50,000 cells/well in a 24 well plate. Hydrogel conditions consisted of either native collagen (NC) or IKRG grafted collagen in different ratios. Different concentrations of peptide-grafted collagen were tested by mixing separately prepared hydrogel suspensions of grafted collagen and native collagen in specific ratios. IKRG-100 represents a hydrogel made entirely of the grafted collagen whereas IKRG-50 is a 50:50 mixture of IKRG grafted collagen:native collagen. Soluble BDNF and IKRG controls were carried out by introducing BDNF and IKRG to the culture media of cells seeded onto native collagen hydrogels. Cells were cultured in neurobasal medium (Life Technologies) supplemented with 2% B-27 Supplement, 1% KCl, 1% Pennacillin/Steptomyocin, and 0.5% L-glutamine. Cells were maintained for 7 DIV before fixation with 4% paraformaldehyde and then stained immunohistochemically with chicken anti βIII-tubulin (Aves) followed by goat-anti-chicken AlexaFluor 568 secondary antibody (Life Technologies). Epifluorescent images were taken on an Olympus IX81. Neurite length was measured via ImageJ.

2.2.4 CGN Viability and Metabolic Activity on Peptide Grafted Collagens

CGNs were seeded either directly onto PLL coated tissue culture well plates or on top of collagen hydrogel conditions at 50,000 cells/well in a 48 well plate. Cells were maintained in culture for 1, 3, or 7 days after which cell viability was quantified using a Live/Dead Cell Viability Kit (ThermoFisher) per the manufacturer's instructions. Epifluoresent images were taken on an Olympus IX81 and cells were counted using ImageJ. Viability was reported as the number of viable cells divided by the total number of cells. Cellular metabolic activity was evaluated on days 1 and 3 using the Vybrant MTT assay (Life Technologies) according to the manufacturer's instructions.

2.2.5 Glutamate Induced Excitotoxicity

CGNs were cultured on poly-L-lysine (PLL) coated tissue culture wells at ~2,000,000 cells/mL. Cytosine β-D-arabinofuranoside (Ara-C) was added to the cultures on DIV 2 to inhibit proliferation of astrocytes. Glutamate injury was induced on DIV 9 by adding 300µM or 500µM glutamate to neurons for one hour. Recovery treatments were added to the wells and incubated for 24 hours. Cellular metabolic activity was assessed immediately following recovery treatments using an MTT assay. Recovery treatments included IKRG grafted collagen (IKRG-100), a 50/50 mixture of IKRG-grafted and native collagen (IKRG-50), and native collagen at 0.33mg/mL, soluble IKRG peptide at 1µM, and soluble BDNF at 10ng/mL.

2.3 RESULTS

2.3.1 Neurite Outgrowth on Peptide Grafted Collagen Hydrogels

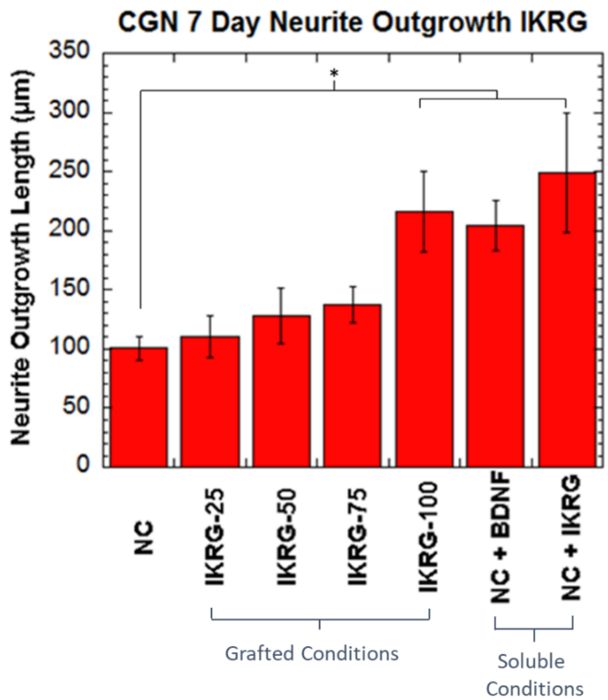

Figure 2.1: Neurite Outgrowth from IKRG Grafted Collagen Hydrogels. IKRG grafted collagen hydrogels promoted enhanced neurite outgrowth in cultures of cerebellar neurons. Further, the effect increased with increasing concentrations of grafted IKRG in grafted hydrogel conditions. IKRG-100, native collagen (NC) + soluble BDNF, and native collagen + IKRG conditions showed significantly longer neurite outgrowth than native collagen.

CGNs were seeded on top of collagen hydrogels conditions and cultured for 7 days. As can be seen in Figure 2.1 neurites extending from CGNs cultured on IKRG-100 gels as well as soluble IKRG and BDNF conditions were significantly longer than neurites observed on native collagen gels ($P < 0.0015$). Further, increasing amounts of grafted IKRG peptide corresponded to an increase in neurite length.

2.3.2 Cellular Viability on Peptide Grafted Collagen Hydrogels

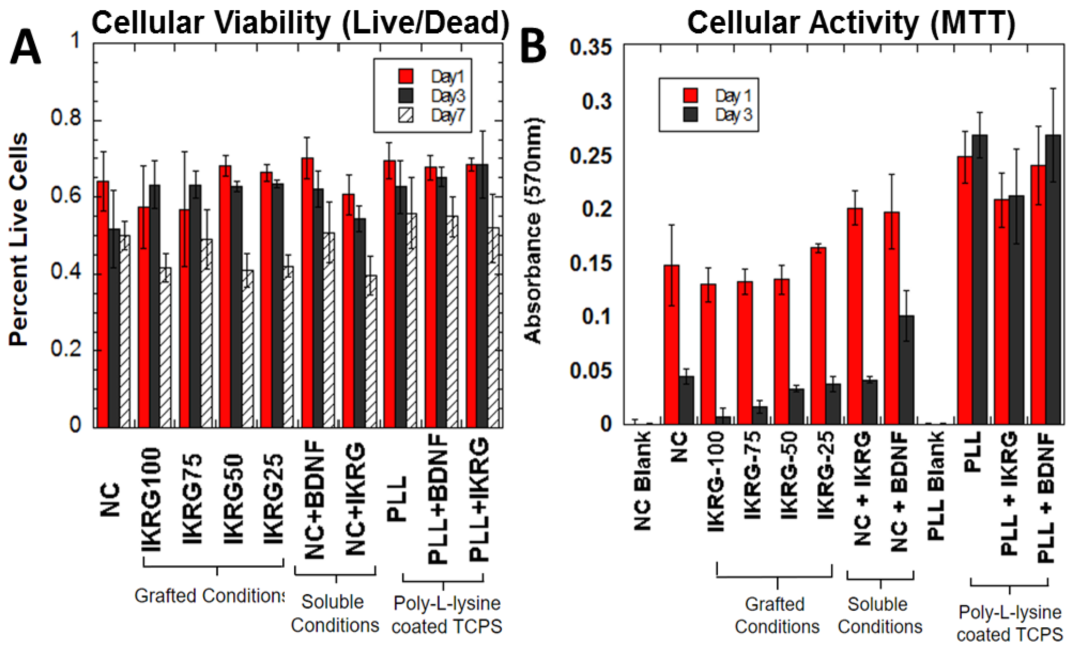

Figure 2.2: Cellular Viability and Metabolic Activity of CGNs Cultured on IKRG Grafted Collagen Hydrogels. Variable viability, metabolic activity, and morphology of CGNs was observed between collagen hydrogel conditions. (A) Cellular viability and (B) metabolic activity of CGNs cultured on IKRG grafted collagen and native collagen hydrogels, compared to CGNs cultured on poly-L-lysine coated tissue culture plastic. +BDNF and +IKRG indicate conditions where soluble BDNF or IKRG was added to the culture media.

There was no observable difference in viability between CGN cultures on the various hydrogel conditions (Figure 2.2A). However, cellular viability is slightly higher on PLL coated tissue culture plastic control conditions when compared to hydrogel conditions, particularly at days 3 and 7. Differences between hydrogel and tissue culture plastic conditions are further evident in cellular activity studies

(Figure 2B). Cellular metabolic activity of CGNs cultured on collagen hydrogels was less than that of CGNs cultured on PLL coated tissue culture well plates, substantially so at day 3. Morphologically there are also differences between CGNs cultured on PLL coated tissue culture plastic and CGNs cultured on collagen hydrogels. CGNs cultured for 7 days in vitro on PLL coated tissue culture plastic exhibit long processes which appear to form a complex, interconnected network. CGNs cultured on hydrogel conditions exhibit processes which do not appear well developed, consisting of shorter neurites which extend towards few neighboring neurons.

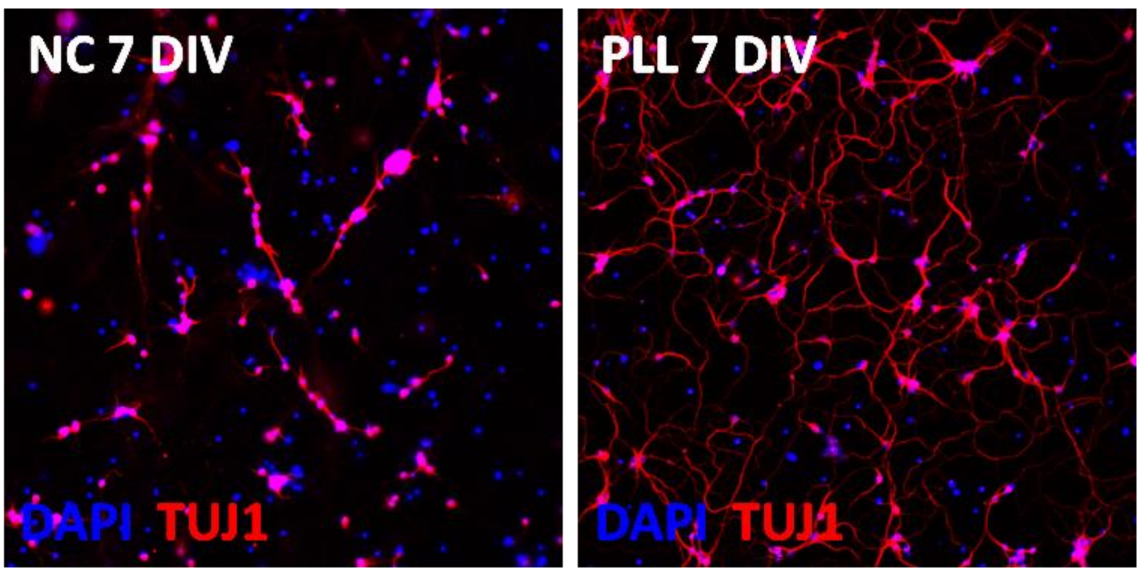

Figure 2.3: Morphology of CGNs Cultured on Native Collagen Hydrogels and PLL Coated TCPS. Immunocytochemical staining of CGNs cultured on native collagen (NC) and poly-L-lysine coated tissue culture plastic (PLL) for 7 days. CGNs were stained for β-III tubulin (TUJ1) and DAPI.

2.3.3 Glutamate Induced Excitotoxicity Results

Glutamate induced excitotoxicity experiments on CGNs were carried out between DIV 9 and 12. CGNs were treated with glutamate to induce excitotoxic injury and then the glutamate was removed and replaced with recovery treatments. In injury only conditions (untreated), metabolic activity was reduced ~60% of uninjured controls. Metabolic activity of native collagen control conditions was lower than the injury only controls (~20-30% normalized metabolic activity). The highest concentration of IKRG grafted collagen (IKRG-100) showed similar metabolic activity to soluble IKRG and BDNF controls (~45-55% metabolic activity), but only slightly higher than untreated conditions.

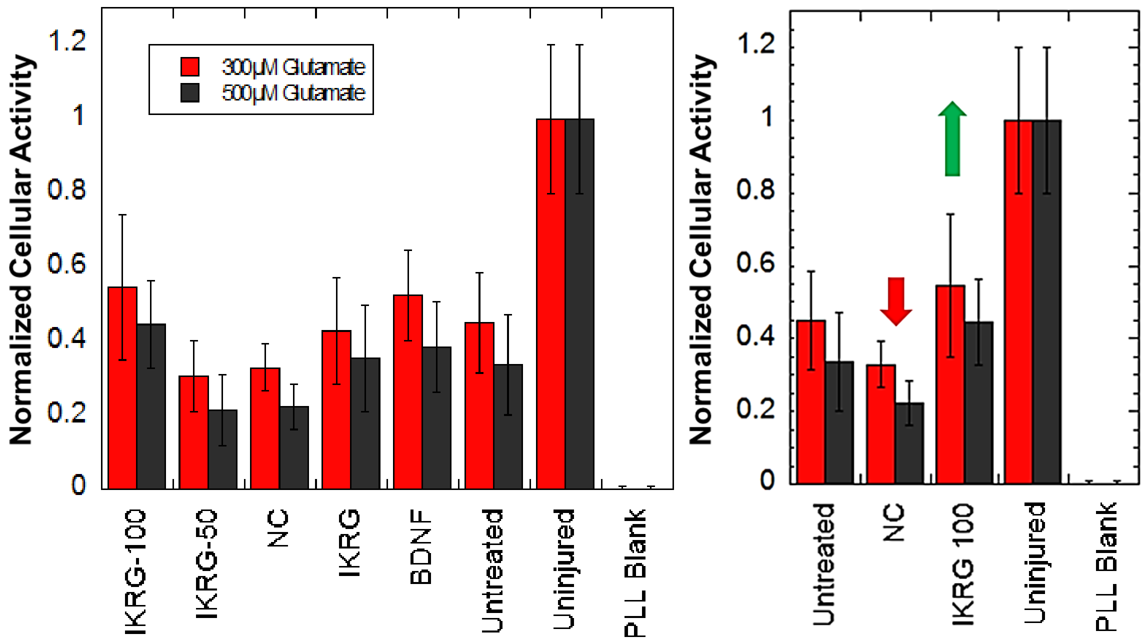

Figure 2.4: Cellular Metabolic Activity Measurements Following Glutamate Induced Cytotoxicity and Recovery Treatments. Cellular activity following glutamate injury and subsequent recovery treatment as measured via MTT. Untreated condition was injured with glutamate but received only culture media during recovery treatment. Different concentrations of IKRG grafted peptide was achieved by mixing separately prepared peptide grafted collagen with native collagen in specific ratios. Soluble Conditions indicates the peptide or BDNF was added solubly to the culture media. Right panel illustrates the conflicting effects of the native collagen and the grafted peptides. All values are normalized to uniniured control.

2.4 DISCUSSION

To confirm the functionality of the grafted peptide, we cultured CGNs on peptide-grafted collagen hydrogels and measured the length of neurites extending from the cell bodies. We hypothesized that CGNs would respond similarly to peptide-grafted collagen hydrogels and soluble BDNF or IKRG peptides. Figure 1 shows measurements of neurite outgrowth from CGNs cultured on the IKRG grafted hydrogels, as compared to native collagen, native collagen with soluble BDNF added to the culture media, and native collagen with soluble IKRG peptides added to the culture media. Soluble BDNF and the soluble IKRG peptide increased the length of neurites. Different concentrations of peptide-grafted collagen were tested by mixing grafted collagen with native collagen. IKRG-100 represents a hydrogel made entirely of the grafted collagen whereas IKRG-50 is a 50:50 mixture of grafted collagen:native collagen. CGNs demonstrated longer neurite outgrowth on IKRG and grafted collagen hydrogels when compared to outgrowth on native collagen controls. Neurites were generally longer on hydrogels with the highest concentration of grafted peptide, which was comparable to both the soluble peptide conditions and the BDNF conditions. These preliminary results indicate that (1) IKRG peptides remain functional following grafting, and (2) there is a functional benefit to covalently incorporating the IKRG peptides into our collagen hydrogels.

Cellular viability studies revealed no observable difference between native collagen conditions and peptide grafted collagen conditions. This suggests that the incorporation of IKRG peptides into the collagen hydrogels does not negatively affect cellular viability. Although live/dead results show that a majority of CGNs may survive on collagen hydrogels, the cellular activity data demonstrates that CGNs on collagen hydrogel conditions are less metabolically active than those cultured on PLL coated tissue culture plastic. The differences are extreme by day 3, with metabolic activity of CGNs on most hydrogel conditions (all except NC +BDNF) is less than 20% the level of metabolic activity observed in the PLL coated conditions. These stark differences between PLL coated tissue culture plastic and hydrogel conditions are mirrored in morphological observations. After 7 days in vitro, CGNs cultured on PLL coated tissue culture plastic display a complex interconnected network of neurons extending long processes to one another. Conversely, CGNs cultured on collagen hydrogels display processes that are much shorter and extend to few neighboring neurons, indicating that these neurons are less well developed. Cumulatively, these results suggest that collagen may be having unintended, effects on the cultured CGNs. These results were taken into account during the design of recovery treatments for glutamate and rotenone injury models.

Glutamate-induced excitotoxicity is a key contributor to cell death resulting from secondary injury following TBI. For this reason, it was selected as a means of modelling secondary injury in vitro, and ultimately to examine neuroprotective potential of the immobilized BDNF fragment peptides in combating the effects of secondary injury. Recovery treatments consisted of grafted and native collagens mixed in specific ratios as described earlier. Instead of forming a gel however, the collagen conditions were added to the culture media at a concentration of

0.33mg/mL. This concentration is too low to form a standard collagen hydrogel, but at physiological culture conditions, individual collagen molecules will self-assemble into fibers. There will not be enough fibers to form a hydrogel, but the fibers that do assemble will be dense so that they sink within the culture wells, sustaining the presentation of the collagen and peptide recovery treatments in close proximity to the CGNs. The goal of presenting the grafted peptides in this manner is to minimize the presence of collagen which appears to be hindering development of cultured neurons.

These grafted collagen conditions were compared to native collagen controls and controls with soluble peptide and soluble BDNF were added to the culture media. Cellular activity was measured via MTT assay and readings were normalized to uninjured control cultures. In the left panel of Figure 4, there seems to be little benefit to our recovery treatments as can be seen when comparing them to the untreated control. Upon closer examination, there may be some confounding factors which are masking potential therapeutic effects. As is illustrated in the right panel of Figure 4, after glutamate injury, we see approximately 60% reduction in cellular activity. Treatment with native collagen *further reduces* the cellular activity of CGNs beyond that resulting from the initial glutamate injury. Treatment with IKRG grafted collagen increases cellular activity nearly twofold above that observed with native collagen, however because of the reduced activity that results from the inclusion of collagen, the overall activity is only slightly greater than the untreated conditions. Based on these observations it is likely that these apparent negative influences of collagen are masking the immobilized IKRG's full potential for neuroprotection. Ultimately this suggests that while there may be some benefit of the immobilized IKRG peptides, collagen is not a positive means of delivering our immobilized peptides in this application. In vivo, collagen is not a component of brain extracellular matrix and the density of neurons and glia is much higher than in culture. It is possible that the CGNs are failing to thrive on the collagen substrates because they are not used to seeing collagen's binding motifs and other bioactive signals that may be unintendedly conveyed by culture on the hydrogel. Their ability to thrive on a bioinert tissue culture well plate with modifications only made to the charge (PLL coating) suggests a bioinert polymer, such as poly-ethylene glycol (PEG), should be employed as the backbone of our proposed immobilized peptide therapeutic.

The primary benefit of collagen in this application is the ability for collagen to self-assemble from a liquid suspension to a fibrillar hydrogel when buffered to physiological pH (7.4) and incubated at physiological temperature (37°C). Through this self-assembly mechanism, the individual collagen molecules undergo a change from low molecular weight species into large molecular weight aggregates. While undergoing this increase in size, simultaneously the speed with which they diffuse is greatly reduced. The initial goal with these peptide grafted collagen hydrogels was to immobilize these grafted peptides to a specific injury site. Collagen's self-assembly mechanism offered the ability to keep the grafted peptide local to the injection site. Based on the apparent negative influence of collagen, an alternative material must be selected as the carrier polymer, but the carrier must also present a means of localizing our therapeutic to the injury site.

2.5 CONCLUSION

Herein we have evaluated the potential of grafting BDNF mimicking peptides to collagen as a way of localizing delivery of peptides to the site of TBI. BDNF mimicking peptides retained their bioactivity following coupling to collagen. Despite this, collagen seems to have had negative unintended consequences on viability of cerebellar granule neurons both in preliminary screening experiments and in glutamate excitotoxicity models. Efforts to minimize these apparent negative effects of collagen were unsuccessful. As such we needed to evaluate alternatives to sustain the presentation of peptide therapeutics to sites of injury or disease.

CHAPTER 3. IMMOBILIZATION OF ACRYLATED POLYMERS VIA NATIVE FREE RADICALS

3.1 INTRODUCTION

As we began to consider alternatives to collagen as a carrier polymer we found inspiration in another modified collagen being developed in our laboratory, collagen methacrylimide (CMA). CMA was created by grafting methacrylic acid groups to lysine residues on the collagen backbone, similar to our synthesis of peptide grafted collagen.[35-36] These methacrylic acid groups can then be crosslinked to one another to increase the mechanical strength of CMA hydrogels. The crosslinking of methacrylic acid groups is initiated by free radicals. We were familiar with free radicals from the CMA project, but also from our research into the pathology of TBI. Elevated concentrations of free radicals are a key contributor to the hostile injury environment that persists after TBI.[37-39] Putting these pieces together, a hypothesis began to form: if free radicals produced on the benchtop can crosslink methacrylic acid groups to one another, can free radicals present in in vivo initiate the same type of crosslinking behavior?

As it turns out, the increased presence of free radicals is not limited to TBI. Elevated concentrations of free radicals are characteristic of a wide variety of tissue injuries and disease states, including inflammatory diseases, neurological disorders, ischemic diseases, burn wounds, cancer, organ transplantation, and traumatic brain injuries.[37, 40-45] Free radicals are species left with at least one unpaired electron, which renders them extremely reactive and capable of causing significant damage to proteins, lipid membranes, nucleic acids, and other critical cellular components. Free radicals that are produced natively in the body include hydroxyl (OH•), superoxide (O2•-), nitric oxide (NO•), and lipid peroxyl (lipid-OO•).[40] Although not free radicals themselves, hydrogen peroxide (H2O2), peroxynitrate (ONOO-), and other species are categorized as oxidants which can mediate free radical reactions or be decomposed into free radicals themselves.[41, 43] Low levels of free radicals are continuously present in vivo and play a crucial role in many cellular functions, such as combating infectious organisms and servicing as messengers in cell signaling cascades.[43, 46] A delicate steady state exists between formation of free radicals in vivo and their detoxification through natural antioxidant mechanisms. In injured and diseased tissues, the production of free radicals is often greatly increased, thereby overwhelming native antioxidant mechanisms and resulting in persistent elevated concentrations of free radicals in afflicted tissues and associated damage.[43]

Although the heightened reactivity of free radicals can be deleterious in vivo, it serves as a valuable tool in polymer chemistry to initiate and control crosslinking or polymerization of a variety of chemical functional groups.[47] Acrylate groups are one type of functional group that are increasingly used in biomedical applications that can be crosslinked in the presence of free radicals.[48] We hypothesized that the elevated production of free radicals in injured and diseased tissues is capable of inducing crosslinking of acrylate groups. If sufficient crosslinking occurs, the polymers will become too large to diffuse out of the tissue, thereby targeting their accumulation as well as any therapeutic factors that are coupled to the original acrylated molecules to the areas of high free radical production. By providing a substrate for the free radicals, these polymers may also provide a measure of free radical scavenging to further protect tissues as an anti-oxidant.

Reaction conditions can be controlled during benchtop chemical synthesis to maximize crosslinking and polymerization efficiency. In contrast, to achieve our stated goal of initiating crosslinking in vivo, we must work within a narrow range of physiologic conditions that we cannot control. To that end a robust characterization of different starting materials and how they react with free radical species commonly encountered in vivo, particularly reactive oxygen species (ROS) and reactive nitrogen species (RNS) is necessary. In this paper, we present a preliminary evaluation of the potential to use ROS and RNS to initiate crosslinking and promote immobilization of acrylated polymers.

3.2 MATERIALS AND METHODS

3.2.1 DPPH Assay

2,2-Diphenyl-1-picrylhydrazyl (DPPH) is a stable free radical with a characteristic purple color. Upon being reduced, the color dissipates, thus the change in color can be used to evaluate the effectiveness of free radical scavengers.[49] Samples of acrylated PEG across a range of molecular weights were dissolved in water at the target concentrations before adding 50µM DPPH in methanol. Thirty minutes after addition of the DPPH to acrylated PEG samples, absorbance at 517nm was measured using a Tecan Infinite M200 Pro.

3.2.2 ROS Reactivity Assay

Generation of ROS was accomplished by combining hydrogen peroxide (H2O2) with horseradish peroxidase (HRP). Using this as a free radical source, the assay was run as a competition between a 3,3',5,5'-tetramethylbenzidine (TMB) substrate commonly used in ELISAs and the acrylated PEG sample conditions. A 50:50 mixture of H2O2 and TMB solution (BD OptEIA TMB Substrate Kit – Fisher Scientific) was combined with the sample condition being evaluated. Lastly, a solution of HRP at 0.1μg/mL was added to initiate formation of ROS. The reaction was allowed to run for 60 seconds before a stop solution of 1M sulfuric acid was added to halt further progression of the assay. Absorbance was read at 450nm and 540nm on a Tecan Infinite M200 Pro. Background signal at 540nm was subtracted from signal at 450nm, per TMB substrate kit instructions.

3.2.3 RNS Reactivity Assay

Interaction of acrylated PEG with RNS was evaluated with the use of S-Nitroso-N-acetyl-DL-penicillamine (SNAP). SNAP is a nitric oxide (NO) donor under physiologic conditions and is used to model the effects of NO in physiologic systems. SNAP was dissolved in phenol red-free Neurobasal media (Life Technologies) and combined with samples of acrylated PEG at target concentrations and then incubated at 37°C and 5% CO2 for 24 hours. Following incubation nitrite concentration was evaluated via the Griess reaction. Samples were prepared by combining 172uL DI water with 63uL of the nitrite-containing sample. This solution was then combined with 20uL of Griess reagent (ThermoFisher). Griess reagent was prepared by combining equal volumes of sulphanillic acid and N-(2-naphthyl)ethylenediamine dihydrochloride per manufacturer's instructions. Solution absorbance was read at 548nm on a Tecan Infinite M200 Pro following 30-minute incubation.

3.2.4 Nuclear Magnetic Resonance (NMR) Spectroscopy Measurements

Polymer samples for NMR were reacted overnight as described in GPC experiments. NMR samples were lyophilized and resuspended in deuterated chloroform. NMR spectra were obtained with a Bruker Avance III 600 MHz.

3.2.5 Size Exclusion Chromatography (GPC) Experiments

Samples of 20mg/mL acrylated PEG of various molecular weight were reacted overnight in PBS with 0, 4, 8, or 12mg/mL HRP in the presence of 80µM H2O2 and 120µM acetylacetone (ROS initiators) or 3mM SNAP (RNS initiator). Following reaction, GPC samples were resuspended in 0.02% NaN3 in 0.5x PBS at 2mg/mL and run through the column at 0.05ml/min. Molecular weight for PEG species was estimated using an EasiVial PEG/PEO, pre-weighed calibration kit (Aligent Technologies). Peak height was used to calculate percent conversion, which was reported as the average of three experiments.

3.2.6 Acrylated PEG immobilization within Collagen Hydrogels

Collagen hydrogels were used as a tissue mimic to evaluate the immobilization of the polymers due to exposure to free radicals. Type-I bovine collagen (Elastin Products Company) was reconstituted in 0.02N acetic acid at 3mg/mL. Buffered hydrogel solutions were prepared using the following protocol for 1ml: 20µL HEPES, 130µL 0.15N NaOH, 100µL 10x PBS, 73µL 1x PBS, and 677µL collagen solution. Two radical sources were investigated. First, for photoinitator conditions, 0.1wt% Irgacure 2959 (BASF), a UV-sensitive photoinitiator, was included in the buffered hydrogel solution. Hydrogel solutions were allowed to self-assemble at 37°C for 2 hours. Acrylated PEG samples doped with 1% v/v 2,000 Da acrylate-PEG-rhodamine or acrylate-PEG-FITC (Creative PEG Works) were added to the hydrogels and allowed to diffuse throughout the gel overnight. Following hydrogel self-assembly and diffusion of PEG solutions, the hydrogels were exposed to UV light for 5 minutes to initiate formation of radicals from the photoinitiator. Second, for ROS conditions, HRP was added to the buffered hydrogel solution. Following hydrogel self-assembly and diffusion of PEG solutions H2O2 and acetyl acetone were added to the gels to initiate ROS formation and allowed to react for 24 hours. For both free radical types investigated, a series of 5 3-hour washes with PBS were performed after reaction with free radicals. The residual fluorescence of the hydrogels after all washes were measured (Rhodamine: excitation 540, emission 568; FITC: excitation 495, emission 525) using a Teacan Infinite M200 Pro Plate Reader.

3.2.7 Rat Dermal Fibroblast Culture and Cellular Protection Studies

Rat dermal fibroblasts (RDFs) that constitutively expressed green fluorescent protein (GFP) were isolated from a transgenic animal (a gift from the W.M. Keck Center for Collaborative Neuroscience) and used to evaluate any cytotoxic effects from the acrylated polymers as well as the potential for reactions of the polymer s with free radicals to protect the cells from oxidative damage. RDFs were cultured in DMEM containing 10% FBS, 1% L-glutamine, and 1% penicillin/streptomycin and seeded onto 96 well plates at a density of 1,500 cells/well. For cytotoxicity studies, acrylated PEG treatments were dissolved in fresh culture media, then added directly to RDF cultures and allowed to incubate for 24 hours. Cellular metabolic activity was then evaluated using the Vybrant MTT assay (Life Technologies) according to the manufacturer's instructions. For cellular protection studies, acrylated PEG treatments were added simultaneously with 600µM H2O2 and allowed to incubate for 24 hours. Metabolic activity was again measured using the MTT assay.

3.2.8 Rat Cortical Neuron Culture and Cellular Protection Studies

Rat cortical neurons were isolated from a timed pregnant animal at embryonic day 18 as described in the literature via techniques previously used in our laboratory.[50] Neurons were cultured in Neurobasal media containing 2% B27 supplement, 1% KCl, 1% penicillin/streptomycin, and 0.5% L-glutamine and seeded into 96 well plates at a density of 100,000 cells/well. For cytotoxicity studies, acrylated PEG treatments were dissolved in fresh culture media without

B-27 added, then added directly to cortical cultures and allowed to incubate for 24 hours. Cellular metabolic activity was then evaluated using the Vybrant MTT assay (Life Technologies) according to the manufacturer's instructions. For cellular protection studies, acrylated PEG treatments were added simultaneously with 20µM H2O2 or 10µM H2O2 and allowed to incubate for 24 hours. Metabolic activity was again measured using the MTT assay.

3.3 RESULTS

3.3.1 DPPH Assay

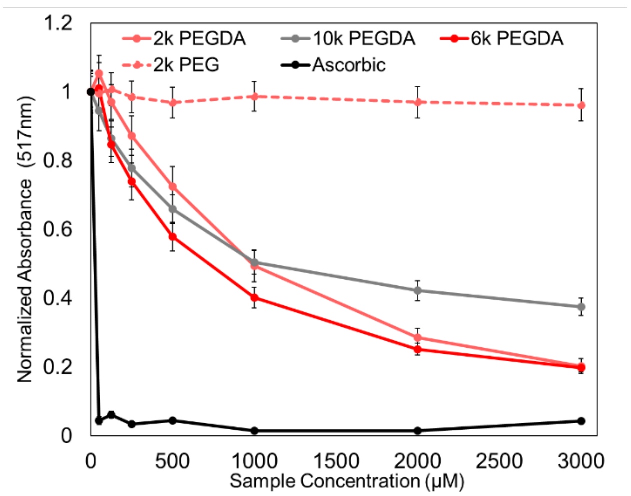

Figure 3.1: Absorbance Measurements from DPPH Assay Following Treatment with Acrylated PEGs. Increasing amounts of acrylated PEGs decrease the absorbance of DPPH, whereas nonacylated PEGs do not. Ascorbic acid is included as a positive control and substantially reduces DPPH absorbance even at low concentrations.

DPPH is a stable radical with a characteristic purple color and a peak absorbance at 517nm. Upon reduction, DPPH loses its purple color and commensurate absorbance at 517nm. Thus, changes in absorbance at this wavelength can be used to monitor the oxidative state of DPPH. Ascorbic acid, a known antioxidant and free radical scavenger, reduced the concentration of DPPH radicals to less than 10% of initial levels, even at very low concentrations. Acrylated PEG across a variety of molecular weights also reduced the absorbance of the DPPH molecule. The highest concentrations of PEGDA examined reduced DPPH to 20-40% of initial levels. When non-acrylated PEG was reacted with DPPH, absorbance of the DPPH molecule remained unchanged, regardless of the concentration of PEG added.

3.3.2 ROS Assay

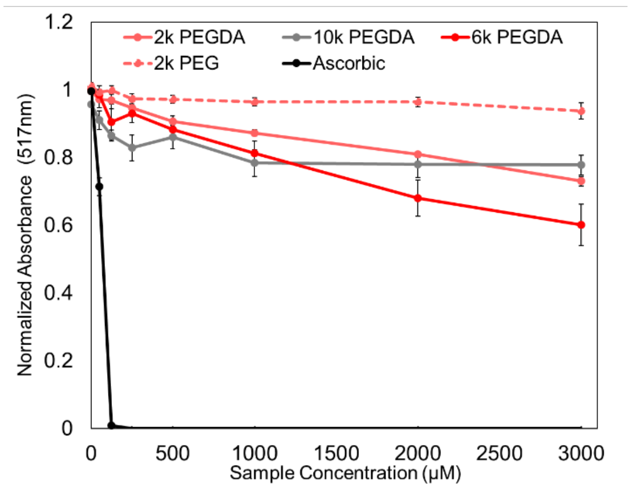

Figure 3.2: Absorbance Measurements from ROS Assay Following Treatment with Acrylated PEGs. Increasing amounts of acrylated PEGs decrease the absorbance of TMB, whereas nonacylated PEGs do not. Ascorbic

acid is included as a positive control and substantially reduces TMB absorbance even at low concentrations.

Reactivity of acrylated PEG with ROS was assessed as a competition assay with TMB as the alternative substrate. Increasing concentrations of acrylated PEG resulted in decreased color development and lower absorbance. Ascorbic acid reduced the concentration of ROS radicals to negligible levels, even at very low concentrations. Acrylated PEG from 2,000 to 10,000 Daltons reduced the TMB absorbance produced by the ROS radicals by 20-40%. When non-acrylated PEG was reacted with ROS, TMB absorbance was unaffected, regardless of the concentration of PEG.

3.3.3 RNS Assay

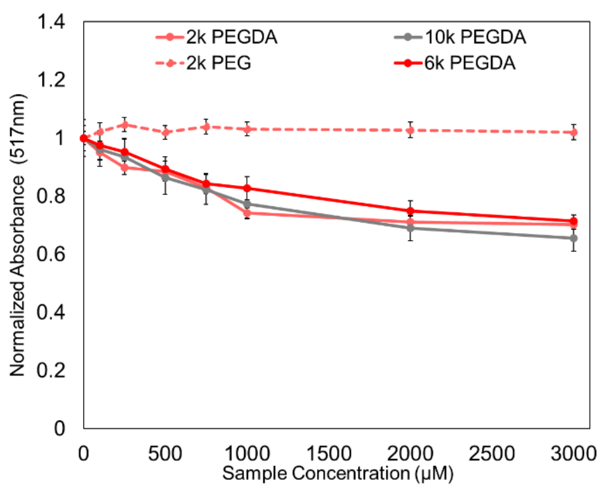

Figure 3.3: Absorbance Measurements from RNS Assay Following Treatment with Acrylated PEGs. Increasing amounts of acrylated PEGs

decrease the absorbance of the Griess reagent, whereas nonacylated PEGs do not. Ascorbic acid was not able to be included because it interferes with the Griess reaction.

Increasing concentrations of acrylated PEG resulted in decreased nitrite concentrations as observed via the Griess reaction. The highest concentrations of acrylated PEG examined resulted in approximately 30% reduction of nitrite concentration across all molecular weights examined. The presence of non-acrylated PEG had no observable effect on the concentration of nitrites. Ascorbic acid has been documented to interfere with the Greiss Reaction, thus ascorbic acid controls were not able to be included in this study.[51]

3.3.4 NMR Spectroscopy

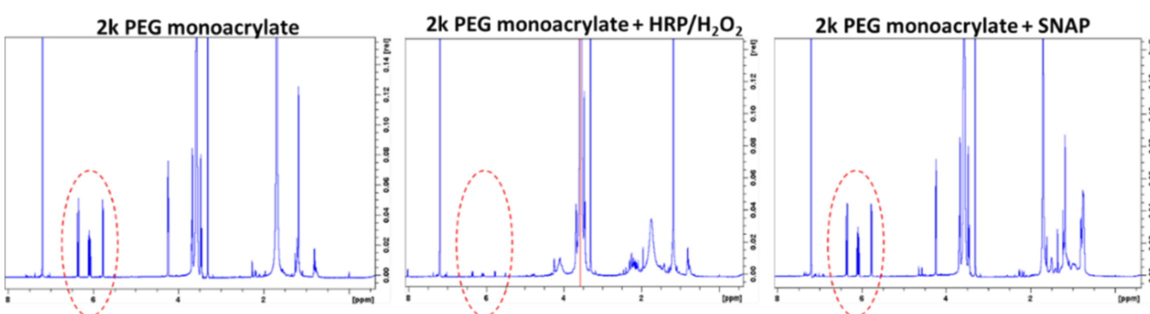

Figure 3.4: NMR Spectra of Acrylated PEGs Treated with ROS and RNS. NMR spectra for 2k PEG monoacrylate (left) shows strong signal from acrylate groups (red dashed circles). After reaction with ROS (middle), the signal from

acrylates is greatly reduced. Conversely, after reaction with RNS (right), the acrylate signal persists unchanged.

Unreacted monoacrylated PEG displayed strong signal from acrylate groups, as observed in the triplet at ~6ppm. After reaction with ROS, the signal from that acrylate triplet was substantially reduced, indicating those acrylate groups have been consumed. Conversely, after reaction with RNS, the signal from the acrylate triplet remains unchanged, indicating that those acrylate groups have persisted.

3.3.5 Size Exclusion Chromatography

PEG (2,000 dalton - 2k PEG), Monoacrylated PEG (2,000 dalton - 2k PEG1A), and Diacrylated PEG (2,000, 6,000, and 10,000 dalton - 2k PEGDA, 6k PEGDA, 10k PEGDA) were reacted with varying concentrations of HRP in the presence of H2O2 and acetylacetone. In the absence of ROS (0mg/mL HRP), a single defined peak was observed, which corresponded to the starting molecular weight of the polymer (2k PEG Mw: 1885, PDI:1.047; 2k PEG1A Mw:1813, PDI:1.053; 2k PEGDA Mw:1779, PDI:1.052; 6k PEGDA Mw:5843, PDI:1.024; 10k PEGDA Mw:10667, PDI:1.019). A peak at ~27 minutes elution time emerges and grows in intensity with increasing HRP concentration as can be seen in Figure GPC A and is present in all PEG sample curves. Analysis of this HRP peak via light scattering estimated the size of this species as ~53,000 daltons using a dn/dc value of 0.185. As HRP concentration increases the intensity of the initial polymer peak decreases. Additionally, the intensity of doublet peaks increases as can be observed in Figure GPC C, D, and E. Changes in peak height were utilized to calculate percent conversion of the polymer as displayed in Table 1.

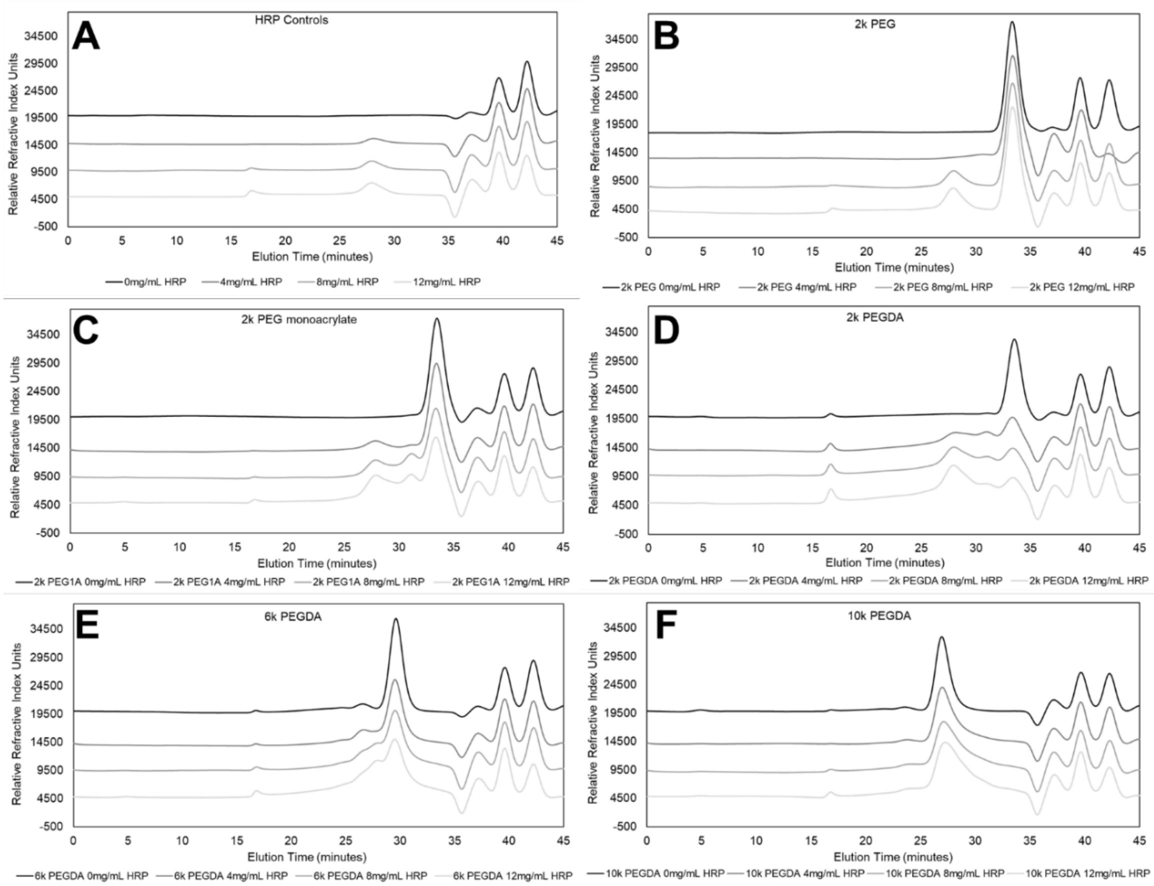

Figure 3.5: GPC Measurements for Acrylated PEGs Treated with ROS. GPC was used to characterize changing size distributions of acrylated PEGs when treated with increasing amounts of ROS. Increasing concentrations ROS were introduced by increasing the amount of HRP present for a given amount of H_2O_2 and acetylacetone. Control curves containing ROS components absent PEGs are presented in frame A. No change in size distribution was observed when non-acrylated PEGs were used (B). Increases in HRP concentration

corresponded to a decrease in the intensity of the initial unreacted polymer peak and a simultaneous increase in the peak intensity of higher molecular weight species for 2k PEG monoacrylate (C), 2k PEGDA (D), 6k PEGDA (E), and 10k PEGDA (F).

HRP Conc.	2k PEG	2k PEG1A	2k PEGDA	6k PEGDA	10k PEGDA
0mg/mL	0%	0%	0%	0%	0%
4mg/mL	2.31% (±4.72)	13.2% (± 3.32)	61.3% (± 2.63)	22.7% (± 7.49)	26.0% (±1.55)
8mg/mL	0.486% (± 5.37)	30.9% (± 3.71)	61.9% (± 6.33)	32.3% (± 3.17)	30.0% (± 3.11)
12mg/mL	4.27% (± 1.83)	32.4% (± 5.67)	62.3% (± 4.69)	31.6% (± 4.88)	29.7% (± 3.07)

Table 3.1: Percent conversion of polymer after reaction with ROS. Percent conversion was calculated by dividing peak height for each concentration of HRP by the peak height at 0mg/mL HRP for each respective polymer and subtracting that from 1, with n = 3. [$Conversion_{nHRP}$=1-($PeakHeight_{nHRP}$/$PeakHeight_{0HRP}$)]

3.3.6 Immobilization Studies

To develop the collagen hydrogel immobilization model, radicals were produced using the photoinitiator Irgacure 2959, which was incorporated into the collagen gel during hydrogel formation. Acrylate-PEG-rhodamine was also included, and the residual fluorescence intensity was read after washing of the collagen gel. Without PEGDA, substantial decreases in fluorescence occurred following UV exposure for PBS and 2k PEG conditions, even prior to washing, presumably indicating destruction of the fluorophore by the free radicals. When PEGDA was included, the decrease in fluorescence as a result of UV exposure was minimal. Following extensive washing, the residual fluorescence for PEGDA conditions was higher than the PBS (not treated) condition. Further, there was an increasing trend between molecular weight of the PEGDA and residual fluorescence – that is, the 10k PEGDA conditions displayed higher residual fluorescence than both the 6k and 2k PEGDA conditions. 6k PEGDA and 10k PEGDA conditions were significantly greater than the PBS (no UV) condition ($p<0.0001$). 2k PEG and PBS conditions displayed low residual fluorescence, due in part to the substantial reduction in starting fluorescence observed after UV exposure but before washing.

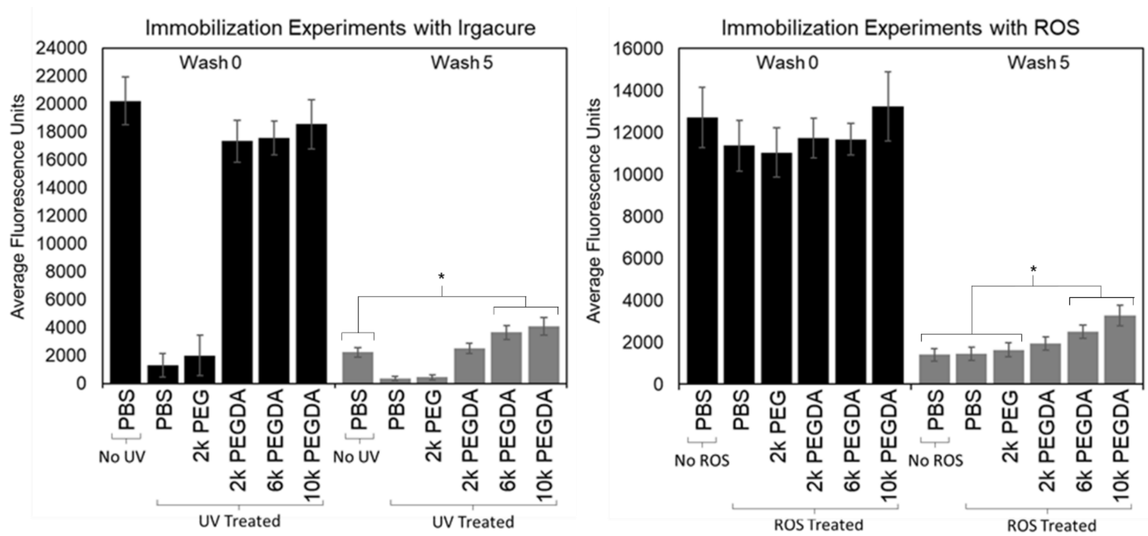

Figure 3.6: Immobilization of Acrylated PEGs within Collagen Hydrogels After Reaction with Free Radicals. Residual fluorescence of hydrogels was measured after reaction with Irgacure radicals (left) and ROS (right). Measurements were taken after reaction with radicals, but before any washes

(Wash 0) and after all washes were completed (Wash 5). Exposure to radicals substantially reduced the fluorescence of rhodamine for Irgacure conditions, even before washes. 6k and 10k PEGDA showed significantly greater residual fluorescence as compared to PBS controls that were not exposed to radicals. For ROS studies, the presence of ROS did not substantially reduce the fluorescence of rhodamine before washes. 6k and 10k PEGDA showed significantly greater residual fluorescence as compared to 2k PEG, PBS, and PBS without radical exposure.

To test the effects of ROS on PEGDA immobilization within the collagen hydrogels, HRP was incorporated into the hydrogel, and H_2O_2 + acetylacetone was added following diffusion of the polymers into the hydrogel. A slight decrease in fluorescence was observed when ROS were produced. Despite this, no conditions were significantly different than PBS without ROS except for 2k PEG ($p=0.0178$). Following all washes, the highest levels of residual fluorescence were observed in conditions with acrylated PEGs. Residual fluorescence for 10k PEGDA and 6k PEGDA conditions were significantly greater than PBS (no ROS), PBS, and 2k PEG conditions. ($p<0.0001$). Residual fluorescence for the 2k PEGDA condition was slightly greater than 2k PEG, but less than that observed for 6k PEGDA and 10k PEGDA.

3.3.7 Cellular Cytotoxicity and Protection Studies

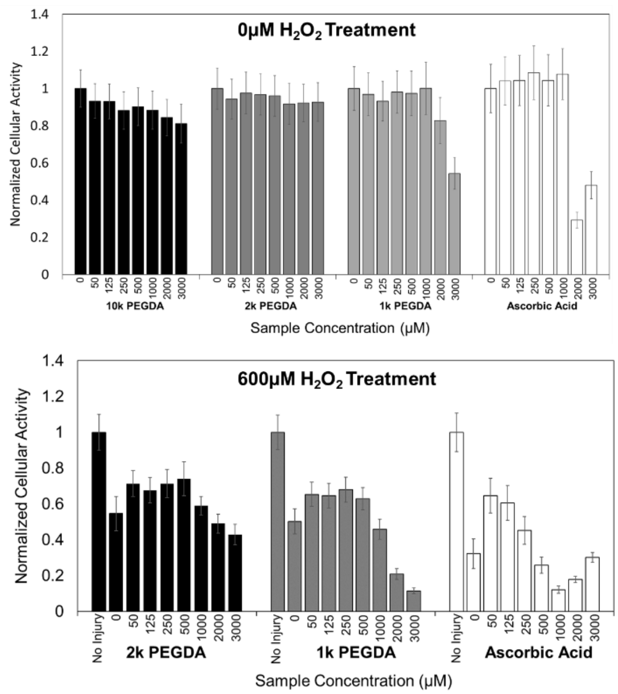

Figure 3.7: Cytotoxicity and Protection of Rat Dermal Fibroblasts. Cellular metabolic activity of rat dermal fibroblasts was assessed in the presence of increasing concentrations of acrylated PEGs and ascorbic acid (top). Cellular metabolic activity of fibroblasts was also measured in the presence of hydrogen peroxide and acrylated PEGs to determine the ability of acrylated PEGs to protect cells from oxidative stress (bottom).

To assess the potential for these molecules to scavenge or otherwise protect cells from oxidative damage, cytotoxicity and cell protection studies were performed. First, the metabolic activity of RDFs and cortical neurons in the presence of acrylated PEGs and ascorbic acid controls was evaluated with the MTT assay without any free radical sources. For acrylated PEG conditions at or below 1,000μM, RDFs maintained greater than 88% of cellular metabolic activity as compared to untreated controls. Acrylated PEG concentrations of 1,000µM and above demonstrated more substantial drop-offs in metabolic activity. These trends were mirrored in ascorbic acid controls; at concentrations less than or equal to 1,000µM, metabolic activity was preserved. Cortical neurons were able to tolerate concentrations of acrylated PEG and ascorbic acid up to concentrations of 500µM without decreases in cellular metabolic activity. At concentrations of 1000µM and greater, cellular metabolic activity was decreased as compared to untreated controls.

In cellular protection assays with RDFs, introduction of 600µM H_2O_2 induced a substantial decrease in cellular metabolic activity when acrylated PEG was not present. Adding increasing amounts of acrylated PEG or ascorbic acid protected RDFs from peroxide injury up to a concentration of 500µM. Concentrations greater than 500µM reduced cellular metabolic activity. For cellular protection studies with cortical neurons, addition of 20µM and 10µM H_2O_2 resulted in approximately 40% and 20% reductions in cellular metabolic activity respectively. Addition of acrylated PEG or ascorbic acid reduced the damaging effects of H_2O_2 up to concentrations of ~250µM. Higher concentrations further reduced cellular metabolic activity.

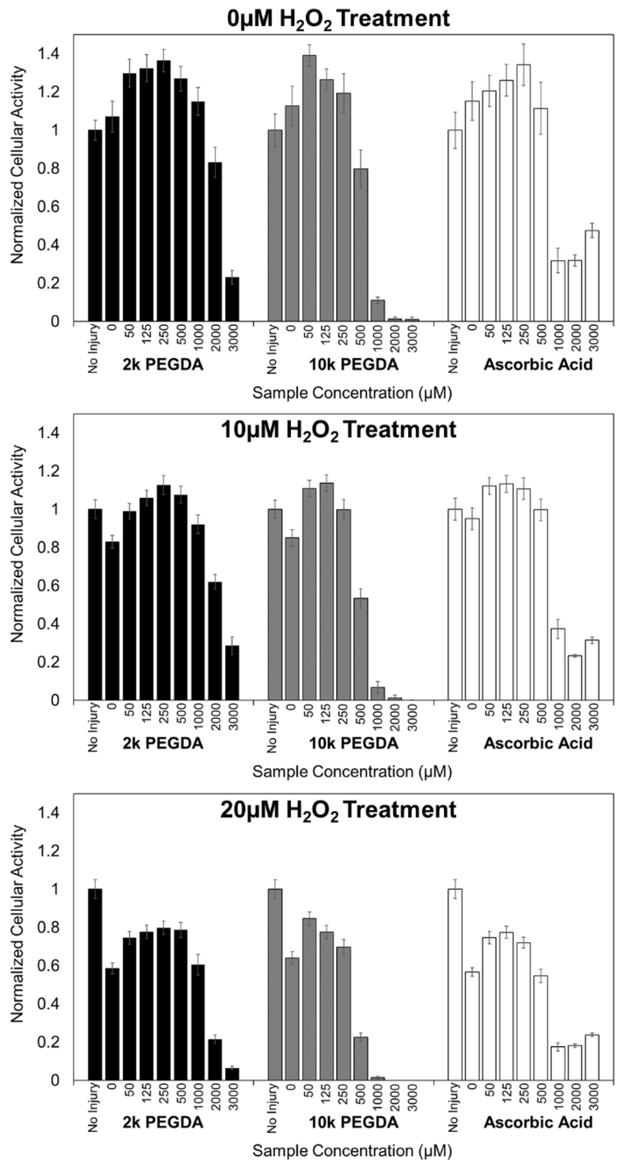

Figure 3.8: Cytotoxicity and Protection of Rat Cortical Neurons. Cellular metabolic activity of rat cortical neurons was assessed in the presence of increasing concentrations of acrylated PEGs and ascorbic acid (top). Cellular metabolic activity of fibroblasts was also measured in the presence of 10μM (middle) or 20μM (bottom) hydrogen peroxide and acrylated PEGs to determine the ability of acrylated PEGs to protect cells from oxidative stress.

3.4 DISCUSSION

Herein, we have demonstrated proof of concept for utilizing native free radicals as a targeting signal to deliver and immobilize therapeutic factors at an injury site. Free radical generators that are commonly used to initiate polymerization and crosslinking reactions in polymer chemistry and biomaterials science typically not compatible with an in-situ assembly approach due to their cytotoxicity. In biomedical applications, UV photoinitiators such as Irgacure are commonly used because they can be used under physiologic conditions, but there are still substantial cytotoxic effects that must be considered.[52] We hypothesized that free radicals that exist naturally in vivo during injury and disease can serve to initiate crosslinking of acrylate groups in situ. We have presented preliminary evidence that (1) acrylated PEGs react with free radicals commonly observed in vivo, (2) the reaction of ROS with acrylated PEGs results in the covalent crosslinking of acrylate groups to one another, increasing their effective size, (3) acrylated PEGs can become trapped within a tissue mimic following reaction with free radicals, and (4) acrylated PEGs can protect cells from oxidative stress in vitro. Collectively, these results represent a positive first step towards establishing a new targeted drug-delivery platform amenable to a wide range of disease and injury states and therapeutic payloads.

The reactivity of acrylated PEG with three different radical species – DPPH, ROS, and RNS – was evaluated with colorimetric assays. Preliminary characterization was performed with the DPPH assay, which is commonly used to evaluate the effectiveness of free radical scavengers. Increased levels of acrylated PEG substantially diminished the number of DPPH radicals present in solution by as much as 80%. Maximum reduction by acrylated PEG was 40% and 30% in ROS and RNS assays, respectively. In all three assays, the presence of non-acrylated PEG had no effect on the concentration of free radicals present, whereas increased amounts of acrylated PEG did reduce the level of radicals present in solution. This confirms that acrylate groups on the PEG chains are responsible for the reactivity with radicals. Although reactive with DPPH and ROS, in neither case did PEGDA reduce the radical concentration as well as ascorbic acid, a well-known, powerful antioxidant. Ascorbic acid controls were not able to be included with the RNS assay due to the strong pH sensitivity of the Greis Reaction. Thus, while the PEGDA may serve as a free radical scavenger, it would not be a primary anti-oxidant.

Though acrylate reactivity with various free radicals was investigated, it was necessary to also confirm that covalent crosslinking of acrylate groups is the result of that reactivity. NMR showed that the signal from acrylate groups was substantially reduced after reaction with ROS, indicating these acrylate groups have been consumed, presumably through crosslinking. In contrast, no change in the NMR spectra was observed following exposure to RNS, suggesting that RNS are not sufficient to induce crosslinking of acrylate groups. Further analysis was done with GPC to monitor the change in polymer size distribution that arises from reaction of acrylated PEGs with ROS. An increase in the molecular weight of acrylated PEGs was observed after reaction with ROS as determined by the emergence of higher molecular weight peaks in the elution spectrum after reaction with ROS. Additionally, there was a concomitant decrease in the intensity of the initial reactant peak, which indicates that the initial, low molecular weight polymer species were being converted into crosslinked, higher molecular weight species. Percent conversion, as calculated from the change in this peak intensity, was dependent on the number of acrylates present and the molecular weight of the staring polymer. The highest conversion was observed for 2k PEGDA (~60%), even when low levels of HRP (and therefore radicals) were present. Larger starting polymers (6k and 10k PEGDA) and monoacrylated polymer (2k PEG1A) showed lower conversion, with all sets topping out at approximately 30% conversion. These results suggest that smaller more mobile PEGs with more acrylate groups are able to react with free radicals more quickly, resulting in more crosslinking events than larger acrylated PEGs. Together, these results demonstrate that native ROS are capable of crosslinking acrylated PEGs. Conversely, consistent with the NMR results, no higher molecular weight peaks appeared in the GPC following reaction with RNS (not shown). Thus, within the range of concentrations studied, ROS, but not RNS, are capable of initiating crosslinking of acrylate groups.

To evaluate the potential for free radicals to crosslink the acrylated PEG sufficiently to immobilize it within a tissue, a collagen hydrogel model was used. Free radicals were introduced to the gels to initiate crosslinking, and an acrylated-PEG fluorophore was included as the payload to allow us to monitor the amount of polymer that remained within the hydrogels. Two free radical systems were used: the photoinitiator Irgacure 2959, to serve as proof of concept for our system, and the HRP-hydrogen peroxide system described earlier. Irgacure 2959 was developed as an efficient photoinitiator for a variety of materials science applications, whereas the ROS system was selected to expose the polymer to free radicals that may be commonly encountered in vivo. The number of radicals produced from Irgacure far exceeds those produced in the ROS conditions, and therefore an increase acrylate-acrylate crosslinking was expected. An unintended consequence of this was the damaging effect of radicals on the fluorescence of the acrylate PEG rhodamine. Following exposure with UV, the fluorescence in non-acrylated PEG and PBS conditions was substantially decreased (Figure 3.6). However, in conditions where acrylate groups were present, very little decrease in fluorescence was observed indicating that the acrylate groups were able to protect rhodamine’s fluorescence by intercepting radicals before they could damage the fluorophore. This speaks to the ability of acrylated PEGs to protect through free radical scavenging. Some fluorophore damage was observed in the ROS system, though to a much lesser degree than in the Irgacure experiments. Because of these differential effects of radicals, raw fluorescence was reported in Figure 3.6 after radical exposure but prior to washing and after extensive rinsing (wash 5).

After reaction with radicals and washing, hydrogel conditions containing acrylated PEGs retained higher levels of fluorescence than PBS or non-acrylated PEG conditions. This suggests that acrylated PEG has become crosslinked within the hydrogel, making it more difficult for the polymer chains to diffuse out of the gel. Sufficient crosslinking will lead to the polymers to form an interpenetrating network trapped within the collagen fibrils. Fluorescence intensity was lower in conditions with non-acrylated PEG or PBS only, demonstrating that increasing the size of the polymer is necessary for immobilization. Further, there was a molecular weight dependence for the residual fluorescence: higher molecular weight acrylated PEGs demonstrated a higher residual fluorescence. In the both ROS and Irgacure conditions, much of the 10k PEGDA was immobilized within the hydrogel, while less of the 6k PEGDA and little-to-none of the 2k PEGDA was immobilized. For 2k PEGDA, each crosslinking event increases the molecular weight by 2,000 daltons. For 10k PEGDA, each crosslinking event increases the molecular weight by 10,000 daltons. Thus, 10k PEGDA conditions will reach an “immobilization threshold” after fewer crosslinking events than the 2k PEGDA. In the ROS conditions, where there are fewer radicals than Irgacure, there was insufficient crosslinking to immobilize 2k PEGDA within the hydrogels. However, in GPC experiments, it was shown that the smaller molecular weight PEGDA had the highest conversion, presumably because the smaller chains were more mobile in solution and could interact with a greater number of radicals before the radicals extinguished. Moving forward, these results suggest a combination of sizes will be most optimal to achieve immobilization of a polymer network within a tissue: small, fast-reacting acrylated chains that will undergo several crosslinking events, and larger chains that will amplify the size increase upon crosslinking.

ROS and RNS generating systems were selected to introduce free radicals on the benchtop that would commonly be encountered in vivo. SNAP presented an especially straightforward method of introducing NO into solutions, as it involves one component, and the donation of NO is achieved by a simple adjustment of temperature and pH. Generation of ROS was less straightforward but achieved through well understood methods commonly used in ELISA assays and enzymatic polymerization.[53-54] Acrylated PEGS were readily able to react with the ROS generated with HRP and H2O2, as seen by the reduction of color development from the TMB substrate, essentially indicating a competition between the acrylated PEG and the TMB. However, for crosslinking to occur, the radicalized acrylated PEG must then engage with another acrylated PEG, and radicals may expire before this second reaction could occur. Our benchtop system delivers a single bolus of ROS. Free radicals are created all at once, and then there is only a short window while those radicals are active that crosslinking can occur. In contrast, in vivo during injury and disease production of ROS occurs continuously and there will be a constant source of free radicals so there will be a continuous opportunity for crosslinking to occur. During this extended window a greater number of radicalized acrylated PEGs will be able to interact and thus a greater number of crosslinking events will be able to occur. To adapt our bolus system, in NMR, GPC, and immobilization experiments, an additional component, acetylacetone, was included to prolong the life of those radicals, ensuring that the ROS remain reactive long enough to initiate crosslinking. Collectively, while these systems do not exactly mimic what occurs in vivo, these results still represent a strong first step in demonstrating that acrylated PEGs can be successfully immobilized by ROS derived free radicals.

In preliminary cytotoxicity studies, RDFs tolerated the presence of acrylated PEGs below concentrations of 1,000µM. At concentrations greater than 1,000µM, the toxicity in acrylated PEG conditions mirrored that of ascorbic acid. Similarly, rat cortical neurons tolerated acrylated PEGs up to ~500µM. Above 500µM, decreases in cellular activity were observed, coincident with decreases observed in ascorbic acid conditions.

In addition to initiating crosslinking, the reaction of free radicals with acrylated PEGs may sequester or otherwise occupy the free radicals to prevent damage to nearby cells and offer a measure of cellular protection. Indeed, without acrylated PEG, exposure to H_2O_2 substantially reduced cellular metabolic activity of RDFs and cortical neurons. When even small concentrations of acrylated PEG was present, that injury was reduced. The positive influence of acrylated PEG was dose-dependent up to ~500µM for RDFs and ~250µM for cortical neurons. Decreasing viability at higher concentrations in protection studies occurred at slightly lower concentrations than in the cytotoxicity studies. We suspect that the additional oxidative stress induced by the H_2O_2 may have made the cells more susceptible to toxicity from the acrylated PEGs. This idea of acrylate-conferred protection was also supported by the apparent protection of fluorophore discussed in the immobilization experiments. Ultimately, this ability of acrylated PEGs to confer additional protection may present the opportunity to ameliorate injured or diseased tissues through multiple independent mechanisms.

3.5 CONCLUSION

Herein, we have presented preliminary support of our hypothesis that acrylated PEGs can be used to target and sustain the presentation of therapeutic factors within injured or diseased tissues. Acrylated PEGs have been shown to interact with ROS and RNS, but it appears that only ROS are capable of successfully initiating crosslinking of acrylate groups to one another. Most importantly, acrylated PEGs were successfully immobilized within collagen hydrogels, demonstrating that there is great potential for acrylated PEGs to serve as a building block for a drug delivery platform which both targets and sustains the presentation of therapeutics to a broad range of injured and diseased tissues. Ongoing and future work aims to identify optimal sizes and configurations of the acrylated carrier polymers and to test these polymers in more advanced tissue mimic models. In addition, we are actively evaluating the efficiency of other free radical sensitive functional groups that may meet or exceed the reactivity of acrylates with ROS and potentially RNS. Ultimately, this proposed system represents a versatile drug delivery platform that targets regions of injured or diseased tissue that could amended to carry nearly endless therapeutic payloads.

CHAPTER 4. ALTERNATIVE CHEMISTRIES FOR FREE RADICAL TARGETING AND IMMOBILIZATION

4.1 INTRODUCTION

For several reasons, acrylated PEGs were selected as a model molecule to evaluate the potential for native free radicals to serve as an effective target for delivery and immobilization of therapeutic drugs. Acrylated PEGs are available commercially in a wide variety of sizes and configurations. They are used widely in biomedical research. Finally, crosslinking of acrylates by free radicals drives PEG hydrogel formation. In Chapter 3, we demonstrated that acrylated PEGs can react with free radicals that are common to injury and disease, that the result of that reaction is the covalent crosslinking of acrylated PEGs to one another, and that acrylated PEGs can become covalently immobilized within a tissue mimic after reaction with free radicals. Together, these results serve as proof of concept for the proposed system. In addition to providing positive first steps, this work also demonstrated the potential benefits of using PEGs of different sizes and configurations. There are other functional groups that react with free radicals, and there also may be great benefit to using functional groups with varying degrees of reactivity.[47] Together, the combination of varied size, varied number of functional groups, and varied functional group reactivity would allow this platform to be tuned across a broad range of tissue, injury, and disease types.

In addition to acrylates, alkenes are another functional group that will react with free radicals and could potentially be used in our system, either with homotypically via alkene-alkene crosslinking or heterotypically with thiols via thiol-ene crosslinking.[47] Alkenes feature double-bonded carbons and alkene-based monomers are commonly used in free radical polymerizations. Thiol-ene crosslinking occurs when the sulfur on a thiol becomes covalently bonded to the carbon of an alkene upon reaction with a free radical. Both thiols and alkenes are found regularly in naturally occurring proteins, which suggests that they may be well tolerated by cells when presented on a biocompatible polymer like PEG. Although both free radical-initiated chemistries seem like attractive new targets for our platform, we must confirm that they are capable of reacting with native free radicals. Herein, we report on our characterization of these alternate chemistries for the proposed targeting and delivery platform, opening the door to further tailor the therapy to specific injury or disease conditions.

4.2 MATERIALS AND METHODS

4.2.1 Reactivity Assays

Functionalized PEGs were purchased commercially from BiochemPEG, including 2,000 Dalton Alkene-PEG-Alkene (PEG dialkene) and 2,000 Dalton Thiol-PEG-Thiol (PEG dithiol). DPPH, ROS, and SNAP assays were carried out as described in Chapter 3 substituting PEG dialkene and PEG dithiol for PEGDA. For evaluation of thiol-ene chemistry, a 50:50 mixture of PEG dialkene and PEG dithiol was used, such that the total moles of functional groups was conserved. For example, if the concentration of polymer being tested was 50µM, the concentration of PEG dithiol used was 25µM and the concentration of PEG dialkene was 25µM.

4.2.2 Size Exclusion Chromatography (GPC)

GPC experiments for PEG dithiol and PEG dialkene were performed as described in Chapter 3. Briefly, samples of 20mg/mL functionalized PEG were reacted overnight in PBS with 0, 4, 8, or 12mg/mL HRP in the presence of 80µM H2O2 and 120µM acetylacetone (ROS initiators). Samples were then diluted 1:10 with column buffer (0.02% NaN3 in 0.5x PBS). For PEG dithiol, an additional control was used containing only PEG dithiol dissolved in PBS and diluted in column buffer. The final polymer concentration of samples run through the column was 2mg/mL. For PEG dithiol experiments with SNAP, culture media (95.5% phenol red free neurobasal media, 2% B-27 supplement, 1% KCl, 1% P/S, 0.5% L-glutamine) was used in place of PBS prior to dilution in column buffer.

4.2.3 Cellular Protection Studies

Cellular protection studies with PEG dithiol and PEG dialkene were carried out with rat cortical neurons as described as in Chapter 3.

4.3 RESULTS

4.3.1 Preliminary Screen with DPPH

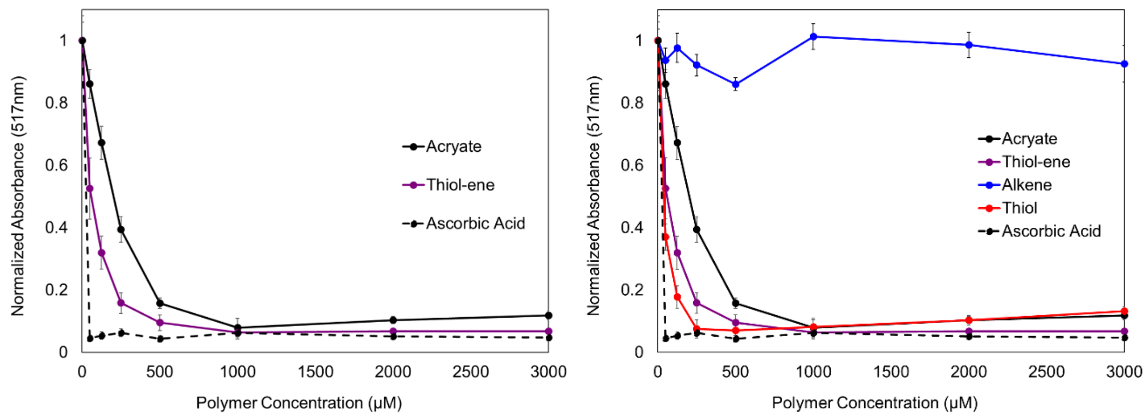

Figure 4.1: Absorbance Measurements from DPPH Assay Following Treatment with Functionalized PEGs. Thiol-ene chemistry was evaluated against acrylated PEG and ascorbic acid using the DPPH assay (left). The thiol-ene chemistry outperformed acrylated PEG and approached reactivity of ascorbic acid. Individual controls for PEG dithiol and PEG dialkene were included in subsequent experiments (right). Thiolated PEGs on their own reduced DPPH absorbance more effectively than thiol-ene. Conversely, PEG dialkene did not appear to substantially reduce the absorbance of DPPH.

The general reactivity of thiol-ene chemistry was evaluated using the DPPH assay. At a concentration of 50µM (the lowest concentration tested) the thiol-ene chemistry reduced greater than 45% of the DPPH radicals, whereas only ~10% of DPPH radicals were reduced by PEGDA. Thiol-ene demonstrated greater reactivity than PEGDA up to ~1000µM, when both curves began to plateau. Characterization of the thiol-ene chemistry was expanded to include their component controls: PEG dithiol and PEG dialkene. PEG dithiol on its own reduced an even greater amount of DPPH radicals than the thiol-ene conditions.

Conversely, the maximum reduction of DPPH radicals observed with the PEG dialkene condition was less than 20%.

4.3.2 ROS Reactivity

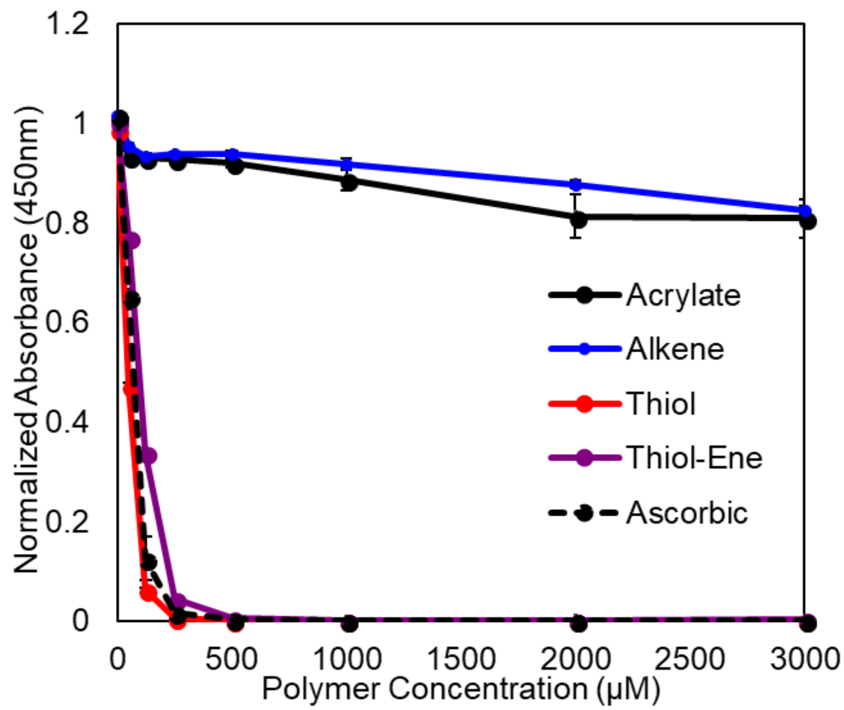

Figure 4.2: Absorbance Measurements from ROS Assay Following Treatment with Functionalized PEGs. Increasing amounts of all functionalized PEGs tested (as well as ascorbic acid) decreased the absorbance of TMB. Thiolated PEGs met or exceeded TMB reduction observed in ascorbic acid conditions. PEG dialkene reduced TMB absorbance to a much lesser degree, but was similar to reduction observed in acrylated PEG conditions.

Reactivity of Thiol-ene chemistry, PEG dialkene, and PEG dithiol was compared to PEGDA and to ascorbic acid. PEG dialkene reduced ~20% of ROS at the maximum concentration tested, similar to PEGDA. PEG dithiol substantially reduced ROS even at very low concentrations; 50µM PEG dithiol reduced the presence of ROS ~50%, and 125µM PEG dithiol reduced the presence of ROS by >90%. At these levels PEG dithiol outperformed ascorbic acid, which is a powerful antioxidant and the positive control. PEG dithiol concentrations at 250µM or greater reduced levels of ROS to indistinguishable levels, similar to ascorbic acid. Thiol-ene conditions also reduced levels of ROS very effectively, but less so than that of the PEG dithiol condition.

4.3.3 RNS Reactivity

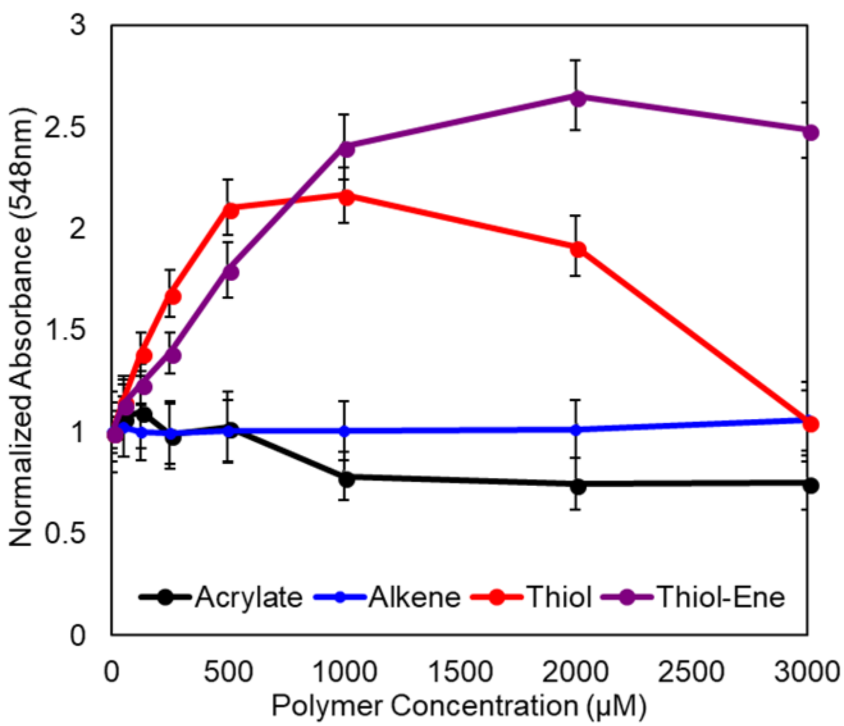

Figure 4.3: Absorbance Measurements from RNS Assay Following Treatment with Functionalized PEGs. Absorbance of Griess reagent

decreased up to ~30% as concentrations of acrylated PEG were increased. Increasing concentrations of PEG dialkene had no effect on the absorbance of Griess reagent. Absorbance for thiol and thiol-ene conditions are skewed by an interfering signal that arises from the interaction of thiols with the Griess reagent. Absorbance for thiol and thiol-ene conditions increased then eventually began to decrease as concentrations of functionalized polymer increases.

PEGDA reduced levels of nitrite by ~30% at the highest levels tested. Levels of nitrite remained unchanged after reaction with PEG dialkene regardless of the concentration used. The presence of cysteines has been documented to interfere with the Griess reaction.[51] This was clearly demonstrated when testing the PEG dithiol and thiol-ene conditions. At low concentrations of PEG dithiol, signal from the Griess reagent increased instead of decreasing. At higher concentrations, the increase in signal tapers off and begins to decrease with increasing PEG dithiol (in both the Thiol and Thiol-ene conditions). The increase and subsequent decrease occurs more quickly in the thiol condition than it does the thiol-ene condition.

4.3.4 GPC Results

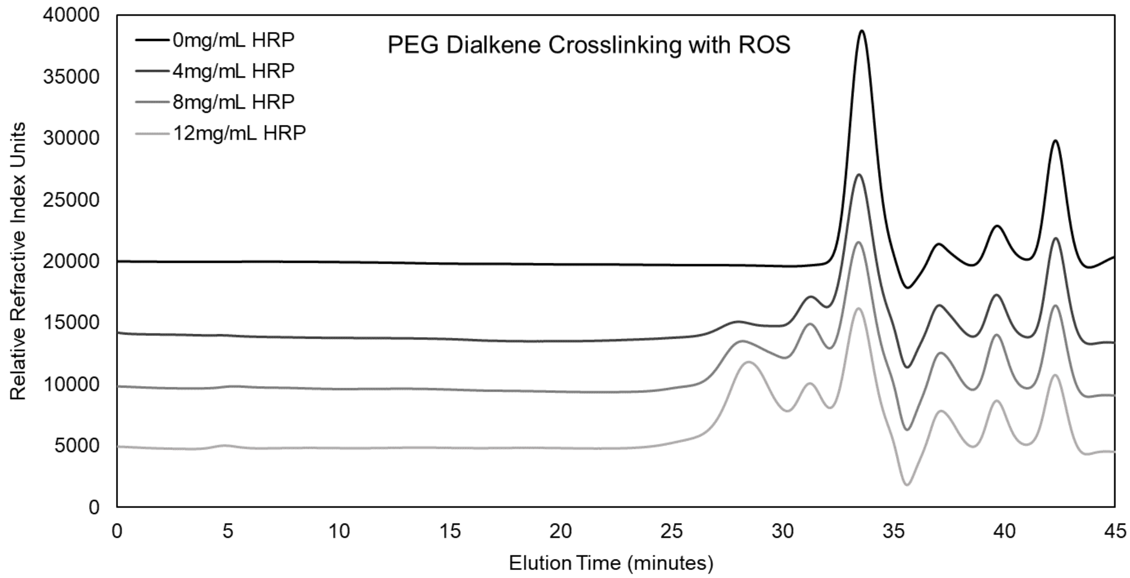

Figure 4.4: GPC Measurements for PEG Dialkene Treated with ROS GPC was used to characterize changing size distributions of PEG dialkene when treated with increasing amounts of ROS. Increasing concentrations ROS were introduced by increasing the amount of HRP present for a given amount of H2O2 and acetylacetone. Increases in HRP concentration corresponded to a decrease in the intensity of the initial unreacted polymer peak and a simultaneous increase in the peak intensity of higher molecular weight species for 2k PEG dialkene.

The crosslinking potential of PEG dialkene in the presence of ROS was evaluated using GPC. In the absence of HRP, a well-defined peak was observed at an elution time of ~33.5 minutes, corresponding to the unreacted PEG dialkene. When the concentration of HRP is increased, the intensity of the unreacted PEG dialkene peak decreases. At the same time, the intensity of higher molecular weight peaks at elution times of ~28 and ~31.5 minutes increase. Percent conversion was calculated by comparing the unreacted PEG dialkene peak height of each concentration of HRP to the peak height of the unreacted PEG dialkene peak at 0mg/mL HRP. Percent conversion of the PEG dialkene was 22.9% (±9.55%) for 4mg/mL HRP, 38.0% (±2.98%) for 8mg/mL HRP, and 44.4% (±7.90%) for 12mg/mL HRP.

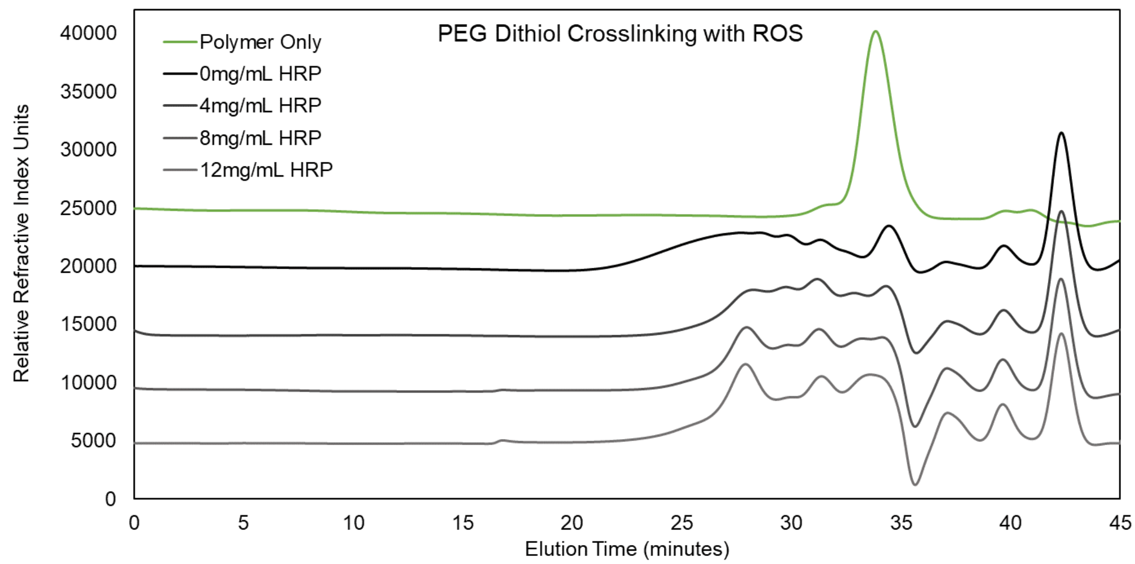

Figure 4.5: GPC Measurements for PEG Dithiol Treated with ROS GPC was used to characterize changing size distributions of PEG dithiol when treated with increasing amounts of ROS. Increasing concentrations ROS were introduced by increasing the amount of HRP present for a given amount of H2O2 and acetylacetone. Increases in HRP concentration showed little change in peak intensity. When compared to a control sample containing only PEG dithiol in PBS (green curve) a much greater intensity peak is observed corresponding to 2k PEG dithiol. When compared to the greys curves, it appears that even small amounts of HRP are enough to induce substantial reduction in peak intensity of the initial 2k PEG dithiol.

The crosslinking potential of PEG dithiol in the presence of ROS was also evaluated with GPC. HRP concentrations from 0 to 12 mg/mL were used to model increasing amounts of ROS. Even at 0mg/mL HRP the intensity of the initial 2k PEG dithiol peak was very low and there was additional signal at earlier elution times, suggesting that crosslinking has already occurred. An additional control was added (Polymer Only), which contained only PEG dithiol dissolved in PBS and diluted in column buffer. This control peak was used as the unreacted reference when calculating percent conversion for the PEG dithiol reacting with ROS. Percent conversion of the PEG dithiol with ROS was 79.5% (±2.54%) for 0mg/mL HRP, 74.9% (±4.93%) for 4mg/mL HRP, 70.2% (±3.09%) for 8mg/mL HRP, and 64.3% (±0.632%) for 12mg/mL HRP.

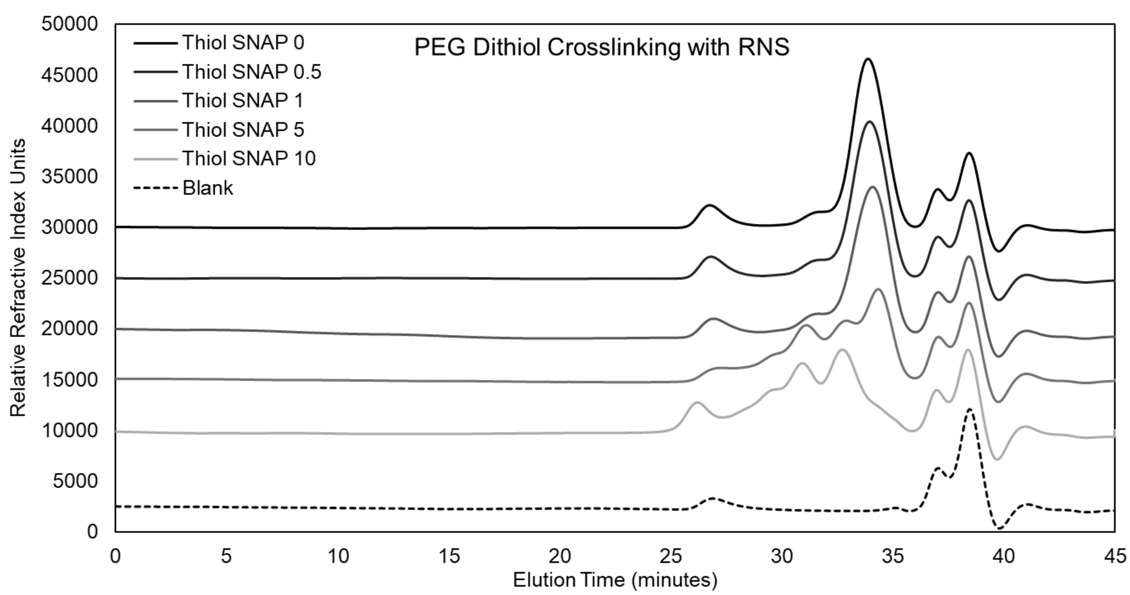

Figure 4.6: GPC Measurements for PEG Dithiol Treated with RNS GPC was used to characterize changing size distributions of PEG dithiol when treated with increasing amounts of RNS. Increasing concentrations RNS were introduced by increasing the amount of SNAP present. Small increases in SNAP concentration

had little effect on the shape of the GPC curves. Larger increases in SNAP concentration showed the characteristic decrease in initial reactant peak intensity and an increase in intensity of peaks for higher molecular weight species. This suggests that RNS are capable of inducing crosslinking of thiolated PEGs.

GPC was also used to evaluate the crosslinking potential of PEG dithiol after reaction with RNS. When low concentrations of SNAP were used, peak intensity changed little. When higher concentrations of SNAP were used (5mM and 10mM) substantial decreases in peak intensity were observed and additional higher molecular weight peaks appeared between elution times of 28 and 33 minutes. Percent conversion of the PEG dithiol with RNS was 4.10% (±4.39%) for 0.5mM SNAP, 16.0% (±5.08%) for 1mM SNAP, 67.8% (±14.6%) for 5mM SNAP, and 81.7% (±1.66%) for 10mM SNAP.

4.3.5 Cellular Protection Studies

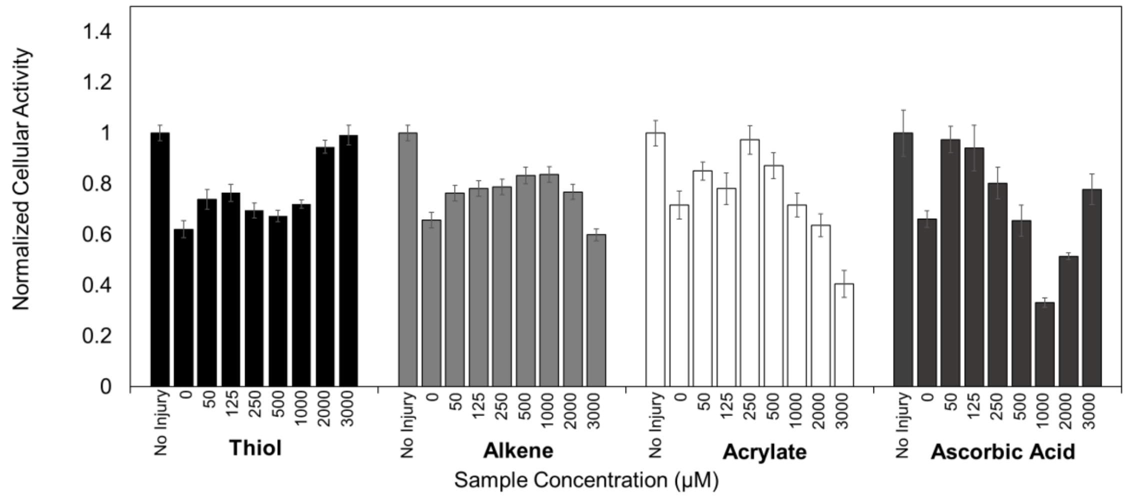

Figure 4.7: Protection of Rat Cortical Neurons via Alternative Chemistries. Cellular metabolic activity of rat cortical neurons was assessed in the presence of 20µM hydrogen peroxide and increasing concentrations of PEG dithiol, PEG diacrylate, PEG dialekene, and ascorbic acid to screen for these compounds ability to protect cells from oxidative stress.

Cellular protection studies were performed with rat cortical neurons. The presence of 20µM hydrogen peroxide induced between 30-40% reduction in cellular metabolic activity. Increasing amounts of functionalized PEGs generally reduced the effects of the hydrogen peroxide induced injury. Introducing PEG dialkene during the exposure to ROS increased the metabolic activity of cells at concentrations up to 1000µM. At concentrations higher than 1000µM PEG dialkene, cells started to show a decrease in metabolic activity. Similar decreases in metabolic activity occurred at 125µM for ascorbic acid and 500µM for PEGDA.

There was some variability in metabolic activity as concentrations of PEG dithiol increased.

4.4. DISCUSSION

The reactivity, crosslinking, and immobilization potential of acrylated PEGs with native free radicals was sensitive to the size, geometry, and number of acrylates present on the acrylated PEGs, as detailed in Chapter 3. This could allow for flexibility in tailoring the proposed drug delivery platform to specific applications. To further expand the range over which this platform can be customized, additional free radical-sensitive functional groups were characterized. Investigation of thiol and alkene functionalized PEGs revealed that (1) thiol and alkene functionalized PEGs met or exceeded the reactivity of acrylated PEGs in assays with native free radicals, (2) reaction with ROS was sufficient to initiate crosslinking of both alkene and thiol functionalized PEGs, (3) RNS were sufficient to initiate crosslinking of thiolated PEG, and (4) cellular protection from oxidative stress was conferred by the presence of thiol and alkene functionalized PEGs. Together these results serve to further expand the utility and flexibility of the proposed native free radical mediated targeting and immobilization platform.

Reactivity assays with DPPH demonstrated that the thiol-ene chemistry substantially outperformed acrylates and even approached ascorbic acid controls in terms of reducing DPPH radicals. This was an overwhelmingly positive result. However, analysis of the results component controls, PEG dithiol and PEG dialkene, suggests that the two components may not be acting together in the manner expected. PEG dithiol on its own reduced DPPH even better than the thiol-ene condition, whereas the alkene conditions showed very little reduction of DPPH radicals. This was also reflected in the ROS assay. The results obtained from the RNS assay were complicated by competing signals induced by the thiols reacting with the Griess reagent, but an interesting trend is observed when comparing the thiol and thiol-ene curves in the RNS reactivity plot. Both curves follow the same general trend, though it appears that the thiol-ene curve is responding more slowly. The absorbance value for thiol-ene at 250µM and 500µM are very similar to the values for the absorbance values for thiol at 125µM and 250µM. The thiol-ene conditions are comprised of 50% thiol which could explain why these values are similar. Together these results all suggest that the thiol-thiol reactivity is the overwhelmingly dominant reaction in thiol-ene conditions. While we initially set out to examine the alkene-alkene (as used to prepare vinyl polymers) and thiol-ene crosslinking, these preliminary results necessitated that we include thiol-thiol crosslinking as well.

Preliminary results for the alkene-alkene conditions in DPPH and RNS showed minimal reactivity. DPPH and nitrite levels remained relatively unchanged, regardless of how much PEG dialkene was present. In the ROS assay, however, PEG dialkene reduced ~20% of ROS, the same amount of reduction observed in PEGDA samples. While this number is low compared to ascorbic acid or PEG dithiol, PEGDA demonstrated strong crosslinking potential and conferred cellular protection from oxidative stress. With similar levels of reactivity in the ROS assay, it is likely that PEG dialkene may also demonstrate similar crosslinking and protection levels, which justified further evaluation.

PEG dithiol results from the RNS assay were complicated by interfering signal arising from thiols being present in the Griess reaction.[51] While the interfering signal seems to obscure meaningful trends for thiol and thiol-ene conditions, the signal may be decomposed into: (1) the absorbance arising from the reaction of the Griess reagent and nitrites (the desired signal) and (2) the absorbance arising from the interaction between thiols and the Griess regent (the interfering signal). At 0µM polymer, the absorbance signal is due entirely to the nitrites present in the solution, since there are no thiols present. Absorbance increased with increasing polymer concentrations up to 1000µM PEG dithiol. In this range, the absorbance signal would be generated by the combination of the nitrites that persist in solution and the interfering signal contributed by the thiol-Griess interaction. At polymer concentrations above 1000µM, the absorbance begins to decrease. One possible explanation for this is that the interfering signal between Griess and thiols has reached a maximum absorbance and adding additional thiol will not increase the interfering signal appreciably. At the same time the thiols have reduced the RNS present, eliminating the desired nitrite signal and causing the total absorbance to decrease. Compiling evidence to support this hypothesis would require extensive further characterization of the Griess-thiol interaction and would deviate from the aims of our work. As it stands, while not conclusive, these results could suggest that PEG dithiols are able to reduce RNS and warranted further investigation through GPC crosslinking studies.

GPC evaluation of PEG dialkene in the presence of ROS demonstrated crosslinking potential similar to PEGDA. As the concentration of HRP is increased, the intensity of the 2k PEG dialkene peak decreases, and peaks corresponding to higher molecular weight species appear, indicating that the 2k PEG dialkene is crosslinking into higher molecular weight chains. Percent conversion for PEG dialkene steadily increased as HRP concentrations increased but was less than the percent conversion observed for PEGDA at the same molecular weight. These results demonstrate that PEG dialkene can crosslink upon reaction with ROS, but that alkenes are less reactive than acrylates.

GPC studies for PEG dithiol with ROS suggested that crosslinking occurred even in the absence of HRP. HRP concentration has been used in our other studies to control the amount of free radicals present given a constant concentration of hydrogen peroxide. Hydrogen peroxide alone appeared sufficient to crosslink the PEG dithiol. This was confirmed by adding an additional control containing only PBS and PEG dithiol diluted in column buffer. When hydrogen peroxide was left out of the solution, a single well-defined PEG dithiol peak was observed. This peak was used as the reference for percent conversion calculations. The amount of hydrogen peroxide in solution is sufficient to convert ~80% of the PEG dithiol in the absence of HRP. While percent conversion drops slightly as calculated by peak intensity when HRP concentrations are increased, the initial 2k PEG dithiol peak becomes less well defined, while the higher molecular weight peaks become more defined. This suggests that there is likely some additional crosslinking that occurs as HRP is introduced.

The decrease in absorbance observed during RNS reactivity assays, while obscured by some interfering signals, indicate that there may be strong reactivity between PEG dithiol and RNS. While RNS were not able to induce crosslinking of acrylated PEGs, RNS did induce the crosslinking of thiolated PEGs. As the concentration of SNAP was increased, the intensity of the 2k PEG dithiol peak decreased, and higher molecular weight species emerged. This indicates that RNS are capable of inducing crosslinking of thiols.

Preliminary investigation of alternative chemistries in cellular protection studies demonstrate that PEG dithiol and PEG dialkene can protect rat cortical neurons from oxidative stress. Increasing concentrations of functionalized PEGs decreased the effects of hydrogen peroxide injury. Increasing the concentrations of functionalized PEG or ascorbic acid too much eventually led to decreases in cellular activity. While preliminary, it appears that the neurons exhibited different tolerances for the different functionalized PEGs. For example, PEG dialkene was well tolerated at concentrations of 1000µM and lower, which was a higher threshold than for ascorbic acid or acrylated PEG. Further, the highest concentrations of PEG dithiol yielded the highest metabolic activities of all dithiol conditions. These preliminary results should be expanded to include additional cell types, but it may allow further tuning of the proposed drug delivery system for specific tissue types or injury and disease presentations.

4.5. CONCLUSION

Our characterization of acrylated PEG indicated that it was well suited as a building block for the proposed native free radical mediated targeting and immobilization platform. Differential reactivity was observed based on polymer chain length or number of functional groups present, but an additional avenue of customization could be added, by including different types of functional groups. Characterization of thiols and alkenes has revealed that both may be suitable for expanding the useful range of our platform. Alkenes were capable of reacting with ROS, and ROS could initiate crosslinking of PEG dialkene, though conversion was less than that observed in previous studies with acrylated PEGs. While PEGDA showed low levels of reactivity with RNS, PEG dialkene showed no ability to react with RNS. In contrast, thiolated PEGs showed very high reactivity with ROS. PEG dithiol was extremely sensitive to ROS, as even decomposition of the hydrogen peroxide in the absence of HRP was enough to initiate crosslinking of ~80% of available thiolated PEG. Further, RNS were capable of initiating crosslinking of thiolated PEG, something not observed in previous studies with arylated PEG. Both groups were also able to confer some degree of cellular protection from oxidative stress. Together these additional functional chemistries greatly expand the range of our proposed therapeutic delivery system. It also opens the possibility that additional free radical functional groups could be applied to our platform in the future as well.

CHAPTER 5. CONCLUSING REMARKS AND FUTURE DIRECTIONS

5.1 THESIS SUMMARY

As the number of complex protein therapeutics available to patients continues to increase, improved means of delivering and sustaining therapeutic concentrations of these medicines are needed. Covalent immobilization of drugs to a polymer backbone can aid in resisting clearance, prolonging presentation of the drug, but a means of localizing these coupled therapeutics to damaged or diseased tissues is needed. Herein, we have demonstrated proof of concept for a native free radical mediated targeting and immobilization platform that can be applied to a wide array of therapeutic factors and applied to dozens of different disease or injury states.

Chapter 2 focused on our efforts to develop a peptide grafted collagen hydrogel to improve regeneration following TBI. Grafted neurotrophic peptides showed promising activity, increasing the neurite length of cultured neurons. However, collagen exhibited a negative influence on cultured neurons, reducing viability and metabolic activity. In glutamate injury models, collagen further exacerbated glutamate injury, working against the potential benefits of the grafted peptides. These results forced us to abandon collagen as a backbone polymer and in doing so, necessitated that we develop an alternative means of immobilizing the backbone polymer and grafted drug within the body.

Chapter 3 detailed our efforts to leverage native free radicals that are present at elevated concentrations in damaged and diseased tissues to target and immobilize drug payloads. While we initially intended to utilize this platform for applications in TBI, there are a plethora of other diseases and tissue injuries which exhibit elevated concentrations of free radicals as a comorbidity. Acrylated PEGs were demonstrated to react with free radicals that are commonly encountered in these afflicted tissues. ROS were capable of crosslinking acrylated PEGs to form higher molecular weight species, and when those chains grew to a sufficient size, they became immobilized within tissue mimics. Ultimately the ability for these acrylated PEGs to react with native free radicals and become immobilized within a tissue is dependent on the size and number of acrylate groups present. Optimal results will likely be observed with a mix of sizes and number of functional groups are employed together. These results demonstrate that acrylated PEGs can be employed as a building block for a drug delivery platform which targets native free radicals and accumulates drug within damaged or diseased tissues where it is needed most.

Chapter 4 expanded the positive results observed with acrylates in Chapter 3 to characterize the reactivity of other functional groups with native free radicals. Alkene functionalized PEGs were reactive with ROS, but not as reactive as acrylated PEGs. Conversely, thiolated PEGs showed greater reactivity with both ROS and RNS as compared to acrylate groups. Further, RNS were capable of initiating crosslinking of thiol groups, something not observed in studies with acrylate groups. The addition of functional groups that are both more and less reactive than acrylates greatly increases the range of radical concentrations this approach may be applied over and further increases the customizability of the proposed drug delivery platform.

Utilizing native free radicals as a signal to target and immobilize therapeutics to injured and diseased tissues may provide the opportunity to improve dosing and treatment options available to patients afflicted with countless different conditions. We have accumulated strong proof of concept for this approach, and these results were used to craft a US nonprovisional patent application filed on June 14, 2018 (No. 16/009,033).

5.2 FUTURE DIRECTIONS

While promising results were obtained supporting the feasibility of the proposed platform, future directions to further advance and apply this approach are suggested below.

5.2.1 Immobilization of Functional Factors

The next demonstration of this proposed drug delivery platform would be to include a functional therapeutic factor as the payload and demonstrate a cellular response in vitro. A model therapeutic for these purposes may be platelet derived growth factor (PDGF). PDGF is a growth factor which upregulates cell division in a number of cell types, including fibroblasts. Further, PDGF activates a protein cell surface receptor, meaning no cleavage will be required for the PDGF to activate its receptor. PDGF can be covalently functionalized to PEG through methods commonly used for pegylation. Drugs and other therapeutic molecules are frequently functionalized with PEG to improve circulation time within the body without substantial reductions in bioactivity. To model delivery of the acrylate-PEG-PDGF, the immobilization model described in Chapter 3 can be adapted and used to screen for the effects of PDGF. After washing, if PEG-PDGF has been successfully immobilized within the hydrogel, fibroblasts will be able to interact with the PDGF and an increase in proliferation of the fibroblasts should be observed. BrdU will be used to identify cells that are actively proliferating in the different conditions. Ideally, conditions that receive acrylate-PEG-PDGF will show a higher percentage of BrdU positive cells as compared to conditions which received non-acrylated PDGF, as the non-acrylated PDGF will be washed out of the gels before it is able to interact with cells. This is just one proposed method of demonstrating the delivery and effects of a functional therapeutic factor, but it could represent an additional step forward in demonstrating the utility of the proposed drug immobilization platform.

5.2.2 Proposed Animal Studies

Ultimately evaluation of this proposed system under injury or disease conditions in natural tissues will be critical to proving it can be effective. While many avenues could be pursued, two possible animal models have been proposed: (1) an ex vivo burn injury model and (2) an in vivo tumor model.

Free radicals are known to be part of the naturally occurring progression of burn wounds. Dermal burns will be applied to rats by immersion in scalding water. After a period of time, skin will be excised from the animals and incubated with solutions of acrylated-PEG doped with fluorescent-PEG-acrylate. Following incubation, the excised tissue will be washed several times and the supernatant collected. Following washing the excised tissue will be fixed, sectioned, and examined under the fluorescent microscope. Free radicals from the burn injury should induce crosslinking of the acrylated PEG. If sufficient crosslinking takes place, the fluorescent acrylated PEG will become trapped within the excised tissue and fluorescent PEG will be visible in the sections. Fluorescence of the collected supernatants will also be measured to assess how quickly the fluorescent PEG diffuses out of the excised tissue in the presence and the absence of radicals.

A second proposed model to demonstrate localization of functionalized PEGs is through a tumor model in mice. Animals will be injected with tumorigenic cell lines to establish tumor formation. Following maturation of the tumors, acrylated PEG doped with fluorescent-PEG-acrylate will be injected into the animals and allowed to circulate. Following administration of the acrylated PEG, animals will be imaged using in vivo optical imaging though the Rutgers Molecular Imaging Center. The MS FX Pro allows for live fluorescence imaging of small animals which will allow us to visualize the distribution of acrylated PEG within the mice. By using a fluorescent antibody for specific epitopes on the tumor cells, we will be able to determine if the acrylated PEG and fluorescence from the tumor tags are co-localized. If the acrylated PEG and tumors are co-localized this will be strong evidence that the proposed technology can specifically target and become immobilized within a diseased tissue.

5.2.3 Incorporation of Cleavable Linkages

PEG has been used as a model backbone polymer in all studies so far. PEG is an attractive model polymer because it is biocompatible and already FDA approved for many applications. Unfortunately, unmodified PEG is not degradable. For our proposed drug delivery method, we are proposing to accumulate a polymer network and grafted drug within damaged and diseased tissues. While we desire for the drug and polymer network to remain in place during the healing process, afterwards it will be desirable for the polymer backbone to degrade into smaller pieces so that it can be cleared. Additionally, there are certain drugs or therapeutic factors that must cross the cell membrane to act on intracellular targets. For payloads such as these, it would be beneficial to have a degradable linkage between the polymer backbone and the therapeutic factor so the therapeutic can be released locally to the immobilization site.

There are several options for degradable linkages that could be employed. Hydrolytically degradable polymers are hydrolyzed in the presence of water and can be tuned to degrade over specific periods of time. Enzyme cleavable linkages are degraded by enzymes that are produced naturally within the body, such as matrix metalloproteinases (MMP). By utilizing hydrolytically degradable polymers or incorporating MMP cleavable linkages into the polymer network, the proposed targeting and immobilization platform could be made more effective for eventual in vivo use.

5.2.4 Two-Phase Delivery Utilizing Click Chemistries

A future evolution of the native free radical mediated targeting and immobilization platform would shift away from a single stage delivery, where the therapeutic is coupled directly to an acrylated (or otherwise functionalized) polymer, to a two-phase delivery system. In the two-phase system, the acrylated polymers would be delivered first and allowed to accumulate at the injury site when they react with native free radicals as described throughout the preceding chapters. These acrylated polymers will have additional “clickable” functional groups that will not react with free radicals and will remain exposed after free radical crosslinking. The second phase of delivery will consist of the therapeutic of choice covalently coupled to the complementary “click” functional group. Essentially, the first phase delivery assembles a net within the injured and diseased tissue, and then that net captures the therapeutic during the second phase of delivery, leaving it exposed for sustained presentation.

Click chemistries are an attractive class of coupling reactions for this proposed iteration of our platform. Click chemistries are bioorthogonal reactions that are highly selective and can proceed quickly under physiologic conditions. Because these reactions are biorthogonal, they do not interfere with other native processes, which could greatly limit off target effects of our delivered therapeutic. Additionally, a two-phase approach could protect the delivered therapeutic from harsh free radicals initially present in the injury environment and would free up reactive sites in the first phase to improve crosslinking efficiency and accumulation of the polymer backbone.

The results described in this dissertation represent strong proof of concept for using native free radicals as a targeting signal and a means of sustaining the presence of therapeutic factors in injured and diseased tissues. Future experiments using bioactive payloads and planned animal studies with further strengthen this proof of concept. To realize the full potential of the proposed drug delivery platform, further development is necessary. Advancing this technology by including degradable linkages and using a two phase “clickable” delivery method will better adapt this platform for eventual in vivo use. Ultimately, the results presented here and the proposed future directions are positive first steps towards realizing the great potential that the proposed native free-radical mediated targeting and immobilization holds to improve delivery of complex biologic medicines.

APPENDIX I. IMMOBILIZED BDNF FRAGMENT PEPTIDE-GRAFTED HYDROGELS TO PROMOTE NEURAL SURVIVAL & REGENERATION

A.1 INTRODUCTION

Structural anisotropy is a factor in the native function of a variety of biological tissues. Structural alignment imparts necessary mechanical strength to load bearing tissues such as skeletal muscle, cardiac muscle, the smooth muscle lining of blood vessels and intestines, ligaments, and tendons.[55-62] Cell and matrix alignment also provide a guidance field for migrating cells or cell processes, which plays an important role in tissue morphogenesis, wound healing, and tissue regeneration.[63-64] Matrix alignment can also guide tissue regeneration in neural tissues such as the spinal cord and peripheral nerves.[65-66] Tissue engineering strategies that incorporate structural anisotropy are crucial in the development of next generation scaffolds, fabricated from synthetic materials or natural polymers, such as collagen.[67-71]

Collagen is the most abundant protein in the human body and a key component of naturally occurring extracellular matrix (ECM).[72] Type I collagen is easily extracted from animal sources, and can be further processed to produce scaffolds that retain a fibrillar architecture characteristic of native ECM.[73] Further, collagen is degraded and remodeled through natural enzymatic pathways, in contrast to many synthetic polymers that degrade hydrolytically into products that can be cytotoxic.[73-76] Extracted type I collagen is biocompatible, FDA-approved for a number of *in vivo* uses, and supports cellular growth and infiltration.[77-78] At physiological temperature and pH, a solution of collagen triple-helical monomers self-assembles into a network of D-banded, triple-helical fibers surrounding a hydrated solution.[79] This fibrillar collagen network imparts mechanical strength to a gel or tissue, presents cell adhesion epitopes naturally within the matrix, and has the potential to guide cells within the network, similar to the topography of natural ECM. [79-80]

There are many approaches to align collagen for use as scaffolds, which have different advantages and drawbacks. Electrospinning is a relatively simple method that can easily generate highly aligned fiber scaffolds starting with collagen as a base solution. However, the volatile solvents, high shear, and harsh electrical fields have been shown to irreversibly alter collagen's native structure, resulting in denatured, gelatin fibers.[81] Alignment can also be induced by applying an external potential field during collagen self-assembly, such as a magnetic field or an electrochemical pH gradient; however, these methods require highly specialized and often costly apparatus, and as a result are difficult to scale up.[82-83] Several approaches utilize directional freezing and freeze drying to form aligned scaffolds from natural polymers such as silk and collagen.[84-90] Wray et. al used gradient freezing of a silk solution in a mold of arrayed wires to fabricate silk-based scaffolds with tunable porosity, channel architecture, mechanical properties, and degradation rates.[84] Stoppel et al. then demonstrated that these aligned silk-based scaffolds could be combined with cardiac tissue-derived ECM to greatly enhance cellular infiltration and vascularization of the scaffold constructs when implanted subcutaneously in rats.[85] Other work has utilized similar freezing and lyophilization methods to produce collagen based scaffolds with aligned pores. Yannas et. al. have prepared collagen and glycosaminoglycan sponges with axially aligned pores through unidirectional freezing and subsequent lyophilization of a collagen-chondroitin sulfate suspension aimed at scaffolds for nerve regeneration[86-89]. Unlike the methods described herein, this approach does not start with a continuous, entangled network of self-assembled, fibrillar collagen, but rather a mixture of soluble collagen and insoluble collagen fragments. More recent work from the same laboratory has demonstrated that collagen-only scaffolds with axially aligned pores can be fabricated through gradient freezing of an acidified collagen suspension. The setup for fabrication of these scaffolds required a custom built polyethylene mold with copper plugs and precise orientation of the molds to allow gradient freezing[90].

Mechanical forces can also be used to generate alignment. Anisotropic strain will orient the collagen fibers in the direction of the maximum strain, and the strength of the alignment will be dependent on the degree of anisotropy.[91] This alignment is local to the axis of maximum strain, and sections of the bulk gel that are not strained will maintain randomly oriented fibrils. One approach to introduce anisotropic strain is via cell-mediated compaction. Cells are included during the preparation of the collagen gel and allowed to compact the gel by generating traction, constraining the deformation of the gel in some directions but allowing deformation in others. Anisotropic strain develops, which leads to fiber alignment. This alignment is dependent on the cell type, number, and incubation time.[92] Anisotropic strain can also be generated from extrinsically applied mechanical forces. In general, to apply this strain uniformly, repeatedly, and consistently, specialized equipment and apparatus are required, limiting the potential of this method for large scale fabrication of aligned collagen scaffolds.

Herein, we present a simple, alternate method that allows for the rapid fabrication of aligned collagen scaffolds. We hypothesized that, by constraining the shape of a collagen hydrogel to a high aspect ratio vessel during freezing and lyophilization, we could control the direction of gel contraction. The combined effect of the high aspect ratio vessel and the high water fraction of the hydrogel that is removed during lyophilization causes the radial shrinkage to be much greater than the axial shrinkage, which would generate scaffold alignment. This method is different from previous approaches with respect to its simplicity, the mechanism by which alignment is generated, and the presence of a continuous, entangled fibrillar collagen network as a starting material.

A.2 MATERIALS AND METHODS

A.2.1 Scaffold Fabrication

All reagents were purchased from Sigma unless otherwise indicated. Type-I bovine collagen (Elastin Products Company) was reconstituted in 0.02N acetic acid at 3mg/mL. Buffered hydrogel solutions were prepared using the following protocol for 1ml: 20µL HEPES, 130µL 0.15N NaOH, 100µL 10x MEM, 53µL Medium 199 (Life Technologies), 10µL L-glutamine, 10µL penicillin/streptomycin, and 677µL 3.0mg/mL collagen solution. The final concentration of collagen in the buffered hydrogel suspension was 2.0mg/mL. Cylindrical silicone conduits (SmallParts.com) of various diameter (2380 µm, 3175 µm, 4762 µm, and 6350 µm) but the same length (6 cm) were used to ensure a high aspect ratio (minimum aspect ratio, length/diameter, was 9.44). These conduits were filled with hydrogel solution, and the filled conduits were then incubated at 37ºC for 1 hour to allow collagen self-assembly. Conduits were then frozen as described below and lyophilized (VirTis Benchtop K) overnight.

A.2.2 Parameter Variation in Scaffold Fabrication

The effects of several parameters on scaffold features were investigated. To study the effects of the freezing temperature and rate of freezing, fibrillar collagen within silicone conduits were placed in either (1) a -80°C freezer for three hours, (2) a -20°C freezer for three hours, or (3) snap frozen in liquid nitrogen. Freezing rate was not directly controlled. To study the effects of collagen concentration, buffered hydrogel suspensions with final collagen concentrations of 2.0mg/mL, 4.0mg/mL, 6.0mg/mL, or 8.0mg/mL were prepared using the recipe described above with suspensions of type-I bovine collagen in 0.02 acetic acid reconstituted at 3.0, 6.0, 9.0, and 12.0 mg/mL respectively. These buffered hydrogel suspensions were self-assembled within silicone conduits, frozen at -80°C, and lyophilized overnight. To determine the effect of a low aspect-ratio vessel on scaffold fabrication buffered hydrogel solutions were prepared as described above, 500µL was placed in a low aspect ratio vessel (15.6mm diameter wells in a 24 well plate (Fisher)), self-assembled at 37ºC for 1 hour, frozen at -80ºC, and lyophilized overnight. The approximate aspect ratio of these scaffolds from the low-aspect ratio vessel was 0.167. Finally, to determine if collagen self-assembly was required to generate aligned features using this process, scaffolds were fabricated from an unassembled collagen suspension. Cylindrical silicone conduits were filled with buffered collagen solution but not incubated at 37°C. Instead, the filled conduits were immediately frozen at -80°C and lyophilized overnight.

A.2.3 Scanning Electron Microscopy (SEM)

SEM imaging of freeze-dried scaffolds and rehydrated scaffolds was performed to evaluate scaffold features such as topography and alignment of surface features. Freeze-dried scaffolds were sputter coated with gold/palladium (SCD 004, Balzers Union Limited) and imaged via SEM (Amray 1830I, Amray Inc.). To observe the morphology of re-hydrated scaffolds via SEM, freeze-dried scaffolds were hydrated in phosphate buffered saline (PBS) for 30 minutes at 37ºC. Hydrated scaffolds were then subjected to dehydration in a series of solutions with increasing acetone concentration (25%, 50%, 75%, and 95%) for 15 minutes each and then placed in 100% acetone overnight. These samples were then critical point dried (CPD 020, Balzers Union Limited), sputter coated with gold/palladium, and imaged via SEM.

A.2.4 Scaffold Diameter Measurements

To make measurements of diameter, the scaffolds were cut into 1 cm transverse sections and placed into 24 well plates. Bright field montages were obtained at 4x magnification. PBS was added to each well, and the scaffolds were allowed to hydrate for at least 30 minutes. A second series of bright-field montages was obtained at 4x magnification to allow a comparison of scaffold diameter between freeze-dried and hydrated states. Scaffold diameter measurements from these images were made using ImageJ (NIH). Scaffold diameter was measured as the edge-to-edge width of scaffolds.

A.2.5 Feature Size Measurements

The width of individual topographical features on the surface of aligned collagen scaffolds was analyzed from SEM images of the freeze-dried scaffolds. Feature size measurements were made using ImageJ.

A.2.6 Uniaxial Tensile Testing

Two groups of scaffolds were tested to determine mechanical properties. Aligned scaffolds were prepared in 6 cm silicone conduits 3175µM in diameter, self-assembled, frozen and lyophilized as described earlier. Random scaffolds were prepared using the low aspect ratio vessel, self-assembled, frozen, and lyophilized as described in the parameter variation study. Both random and aligned scaffolds examined in tensile testing were prepared from a 2.0mg/ml collagen hydrogel suspension and frozen at -80°C. Aligned scaffolds were cut into 13 mm segments, and random scaffolds were cut into 13 x 2 mm segments. Rectangular pieces of polystyrene with punched holes were used as interface between the scaffolds and the mechanical testing apparatus to prevent slippage of scaffolds during testing. Ends of the scaffolds were sandwiched between two pieces of polystyrene with cyanoacrylate adhesive, leaving a consistent gauge length of 5mm. The adhesive was allowed to dry for one hour before the samples were rehydrated in PBS for at least 30 minutes. A representative image of a mounted scaffold is shown in Figure 5A.

Samples were strained in uniaxial tension on a BOSE Enduratec ELF 3200 (BOSE Corporation, Eden Prairie, MN, USA), and load was measured using a 1N cantilever load cell (Measurement Specialties, Hampton, VA, USA). Hooks were formed from 20G steel wire and used apply strain to the samples via the polystyrene. Samples were strained at 0.5 mm/s (10% s¬-1) until failure. Load and displacement were recorded at 24.4 Hz. Load was converted to nominal stress by dividing the load by the cross-sectional area. For aligned scaffolds, cross-sectional area was assumed to be that of a solid cylinder with diameter equal to that of the scaffold. For random scaffolds, cross sectional area was assumed rectangular and equal to the width times the thickness of the scaffold. The thickness of the random scaffolds was determined using a Kinexus Ultra rotational rheometer (Malvern Instruments). Samples were laid flat on the bottom plate of the rheometer stage and the cylindrical upper top plate was lowered until 1.5mm above the bottom of the stage. The top plate was then lowered until a 100 mN normal force was developed, and the thickness of the random scaffold was taken to be the distance from the bottom plate to the top plate.

Ultimate tensile strength (UTS) and strain at UTS were determined. Elastic modulus (E) was taken to be the slope of the linear region of the stress-strain curves, determined using linear regression in MATLAB.

A.2.7 Rat Dermal Fibroblast Culture

Rat dermal fibroblasts (RDFs) that constitutively expressed green fluorescent protein (GFP) were isolated from a transgenic animal (a gift from the W.M. Keck Center for Collaborative Neuroscience). RDFs were cultured in DMEM containing 10% FBS, 1% L-glutamine, and 1% penicillin/streptomycin. RDF’s were seeded directly onto hydrated aligned scaffolds and hydrated random scaffolds formed in low aspect ratio vessels, at a density of ~80,000 cells/cm^2, and maintained in culture for 2 days prior to epifluorescent imaging on an Olympus IX81. The alignment of cells was measured by finding the cosine of the angle between the major axis of the cell and the prevailing orientation of the scaffold features. The major axis of the cells was determined using the entire cell as visualized by the epifluorecent images. These values were squared to produce an alignment index, $\Phi = cos^2\theta$, for each cell, where $\Phi = 1$ indicated alignment parallel to the features and $\Phi = 0$ indicated alignment perpendicular to the features.[93]

A.2.8 Neural Explant Culture

Dorsal root ganglia (DRG) were isolated from pathogen-free chick eggs at embryonic day 8 (Charles River Laboratories, Cambridge, MA) and cultured in DMEM containing 10% fetal bovine serum (FBS), 1% L-glutamine, 1% penicillin/streptomycin supplemented with 100ng/mL nerve growth factor. DRGs were plated onto hydrated aligned collagen scaffolds as well as hydrated random collagen scaffolds and maintained in culture for 3 days. DRG cultures were fixed in 4% paraformaldehyde solution and then stained immunohistochemically with mouse anti-neurofilament 200 followed by goat-anti-mouse AlexaFluor 568 secondary antibody (Life Technologies). Epifluorescent images were taken on an Olympus IX81.

A.2.9 Statistical Analysis

Data was analyzed with a two-way ANOVA followed by posthoc pairwise comparisons with Tukey's All Pair's Comparisons. Differences were considered significant at $P < 0.05$.

A.3 RESULTS

A.3.1 Scanning Electron Microscopy

SEM revealed a highly aligned, topographical architecture with long range uniformity on the collagen scaffolds. The exterior of the scaffolds appeared as a cable-like group of aligned cylindrical structures (Figure 1B), which was preserved along the length of the aligned collagen scaffolds (Figure 1C). Cross-sections revealed a highly porous interior, which may have given rise to folds and ridges on the exterior surface as the scaffolds contracted during lyophilization (Figure 1D). Scaffolds fabricated from un-assembled collagen suspensions in high aspect ratio cylindrical conduits (Figure 1E) showed a highly porous topography but failed to show any alignment of topographical features. Scaffolds fabricated from self-assembled collagen gels in a low aspect ratio vessel (Figure 1F) similarly did not exhibit any preferential alignment of topographical features.

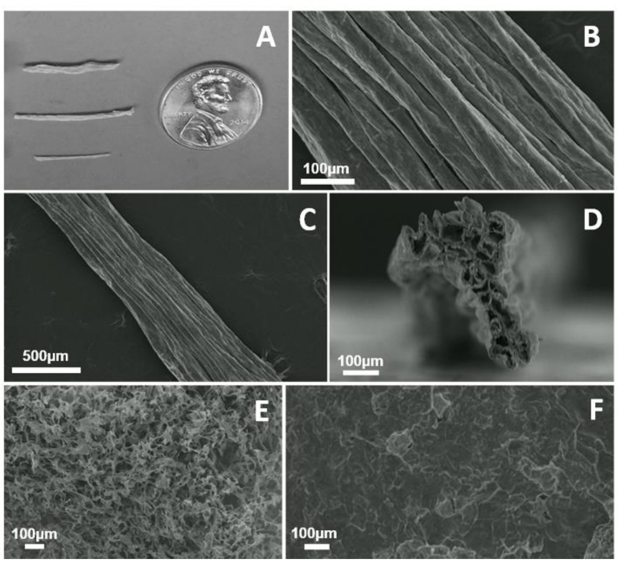

Figure A.1: Example Images of Collagen Scaffold Morphology. (A) Optical image of scaffolds fabricated of various diameters (top to bottom 6350 µm, 4762 µm, and 3175 µm). (B) SEM revealed highly aligned topographical features along the surface of collagen scaffolds. (C) Aligned features were maintained uniformly along the length of collagen scaffolds. (D) Cross sectional SEM images revealed a highly porous interior within the scaffolds. (E) Scaffolds fabricated from unassembled collagen suspensions and (F) scaffolds fabricated from fibrillar collagen in low aspect ratio vessels showed no preferential orientation of topographical features. All samples featured in Figure 1 were fabricated at a collagen concentration of 2.0mg/mL and a freezing temperature of -80°C and were imaged in the dry, as-fabricated state.

A.3.2 Scaffold Diameter Measurements

For scaffolds prepared in the same length of tubing, scaffold diameter after freezing and sublimation was significantly related to the initial diameter for both dry and hydrated scaffolds ($P<0.0001$) (Figure 2A). Post-hoc pairwise comparisons indicated that all scaffold diameters were significantly different from one another ($P<0.0001$) except for the comparison between scaffolds fabricated in the two smallest conduits ($P=0.676$). The collagen concentration also significantly influenced the resulting scaffold diameter for both dry and hydrated scaffolds ($P<0.0001$) (Figure 2B). The effect of freezing temperature on scaffold diameter was also examined (Figure 2C). Significant differences were observed between scaffolds frozen at -20°C and snap frozen in liquid nitrogen in both dry ($P=0.0195$) and hydrated states ($P=0.0074$). Despite this, freezing temperature was not identified as an important factor for determining scaffold diameter, based on the minimal increase in scaffold diameter for a corresponding increase in temperature (Freeze-Dried: 0.53µm/°C; Hydrated 1.62µm/°C). Hydration significantly increased the diameter of scaffolds in collagen concentration and freezing temperature studies (P<0.0001). Hydrating the scaffolds generally increased the diameter of scaffolds in the conduit diameter study, but there was high variability in the final diameter with larger scaffolds, and the increase was not statistically significant (P = 0.059).

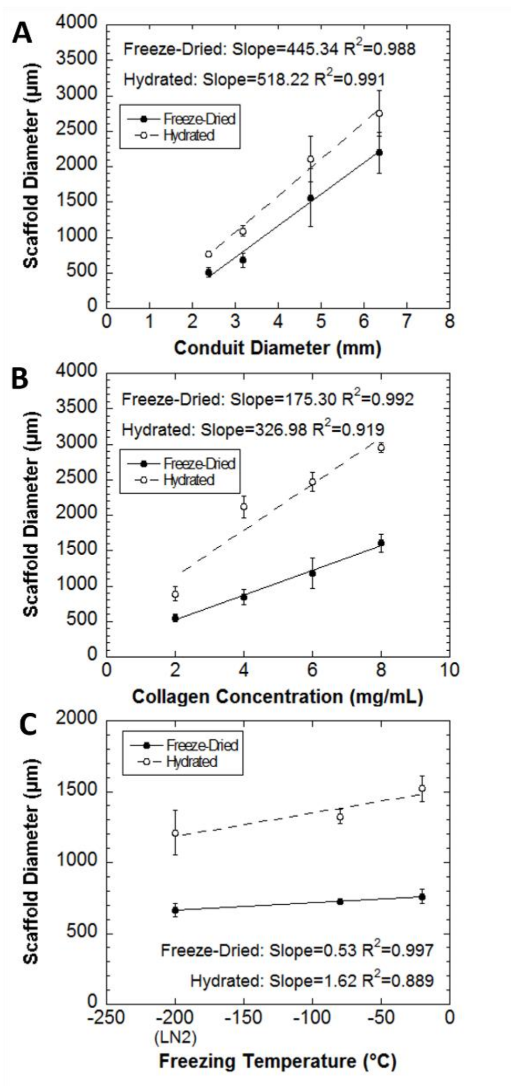

Figure A.2: Scaffold Diameter Measurements Based on Varied Fabrication Parameters. The final scaffold diameter in dry and hydrated states changed with

(A) the initial scaffold diameter, which is the inner diameter of the tube in which the gel is cast; and (B) the collagen concentration of the hydrogel solution ($P<0.0001$). (C) The scaffold diameter varied significantly with freezing temperature in both dry ($P=0.0233$) and hydrated states ($P=0.0088$), with post-hoc comparisons revealing only the differences between scaffolds frozen at -20°C and snap frozen in liquid nitrogen were significant ($P=0.0195$ for freeze dried scaffolds, $P=0.0074$ for hydrated scaffolds).

A.3.3 Feature Size Measurements

The diameter of individual topographical features on the surface of aligned collagen scaffolds was significantly related to the diameter of cylindrical conduits used for fabrication (Figure 3A; $P<0.0001$). However, post-hoc pairwise comparisons indicated that only features from scaffolds made in largest diameter conduits were significantly larger than features from the other conduits ($P<0.0001$). No other comparisons were significant (min $P=0.1868$). The freezing temperature at which scaffolds were fabricated at also significantly affected the diameter of these individual topographical features ($P<0.0001$). However, these factors were poorly correlated (R2=0.577). Snap-freezing in liquid nitrogen resulted in smaller diameter features than freezing at -80 °C or -20 °C (Figure 3B). The concentration of collagen in the initial hydrogel suspension did not have a significant effect on the feature diameter ($P=0.5439$). SEM images of the scaffolds fabricated from collagen assembled in low aspect ratio vessels demonstrated no preferentially aligned or oriented features at any magnification (Figure 1F).

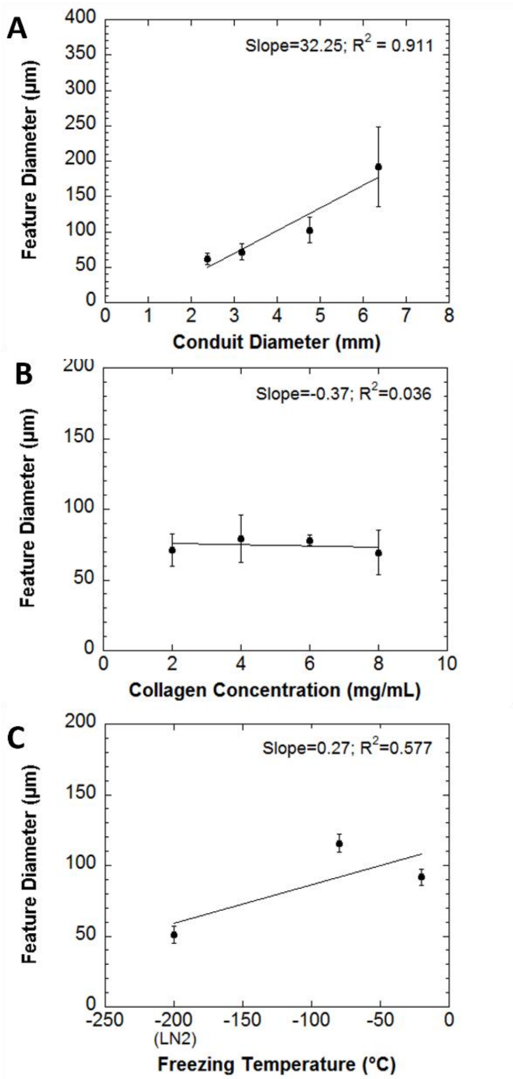

Figure A.3: Feature Size Measurements Based on Varied Fabrication Parameters. (A) The diameter of individual topographical features on the surface of the aligned collagen scaffolds was significantly affected by the initial conduit diameter with post-hoc tests revealing that only the largest conduits produced a significant difference (P<0.0001). (B) The collagen concentration of the hydrogel suspension did not significantly affect the diameter of topographical features (P=0.5439) (C) Freezing temperature significantly affected the diameter of individual fiber-like features (P<0.0001).

A.3.4 Hydrated Scaffold Morphology

Critical point drying of hydrated aligned collagen scaffolds was performed to obtain SEM images of aligned collagen scaffolds in the hydrated state. Critical point drying is commonly utilized to dehydrate biological samples for SEM observation without disrupting the morphology or structure of the sample.[94] SEM of hydrated scaffolds revealed that the aligned topographical features observed in the freeze-dried scaffolds were preserved after scaffold swelling (Figure 4A). At higher magnification, folds and ridges of individual topographical features could be seen that were aligned in the same direction as the larger aligned topographical features (Figure 4B). At greater than 6,500x magnification, randomly aligned collagen fibers were observed, which collectively comprise the larger aligned topographical features (Figure 4, C and D).

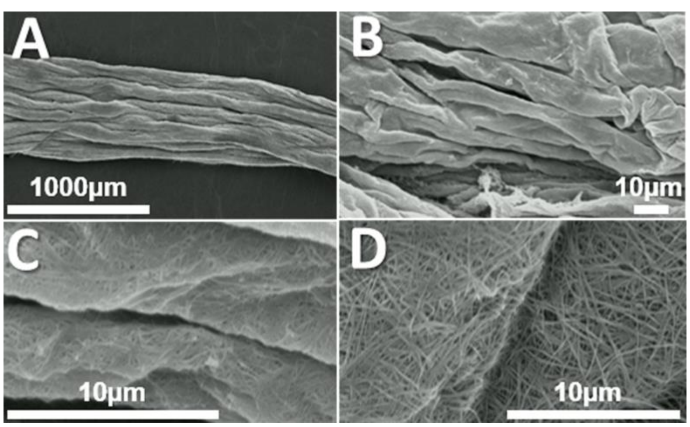

Figure A.4: Representative SEM Images of Aligned Collagen Scaffolds Critical Point Dried in the Hydrated State. (A) Aligned topographical features are preserved in the hydrated state observed at 50X. (B) Folds and ridges of individual features are aligned in the same direction as other scaffold features observed at 1,300X (C) The surface of collagen scaffolds shows evidence of a randomly oriented, fibrillar topography at high magnification. Panels B and C are high magnification frames of Panel A. (D) Representative image showing randomly oriented, fibrillar topography on the surface of a separate collagen scaffold.

A.3.5 Uniaxial Tensile Testing

When strained in tension, the scaffolds displayed non-linear strain-stiffening behavior. A region of nearly elastic deformation is visible on the stress-strain curves after the toe region and before achieving the maximum stress. (Figure 5). Significant differences were observed in scaffold mechanical properties (Table 1). Aligned scaffolds fabricated in high aspect ratio conduits demonstrated a significantly greater ultimate tensile strength than random scaffolds fabricated in low aspect ratio vessels, which displayed no preferential orientation ($P<0.0001$). The strain at the ultimate tensile strength was also significantly greater in aligned scaffolds than in random scaffolds ($P=0.0005$). Differences in elastic modulus were also observed, with aligned scaffolds having significantly greater E than random scaffolds ($P=0.0008$).

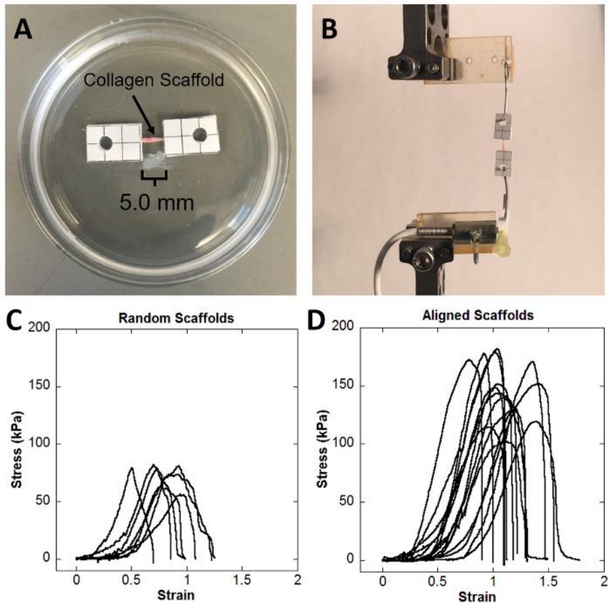

Figure A.5: Stress-Strain Curves of Collagen Scaffolds. Representative images of mechanical testing setup and resulting stress-strain curves. (A) Photograph of aligned collagen scaffold mounted to polystyrene rectangles. (B) Photograph of aligned collagen scaffolds loaded on BOSE Enduratec for tensile testing. (C) Stress-strain curves observed in tensile testing of random scaffolds prepared in low aspect ratio vessels. (D) Stress-strain curves for aligned scaffolds fabricated in high aspect ratio conduits. Both scaffold groups displayed non-linear, strain-stiffening behavior.

Sample	Ultimate Tensile Strength (kPa)	Young's Modulus (kPa)	Strain at UTS
Aligned Scaffolds	147 ± 25.2	567 ± 134	1.10 ± 0.177
Random Scaffolds	73.4 ± 9.91	349 ± 85.5	0.784 ± 0.157

Table A.1: **Mechanical Properties of Aligned and Random Scaffolds.** Ultimate tensile strength (UTS), Young's modulus, and stretch at UTS for aligned scaffolds, fabricated in high aspect ratio conduits, and for random scaffolds, fabricated in low aspect ratio vessels.

A.3.6 Cellular Response to Aligned Scaffolds

Green fluorescent protein-expressing rat dermal fibroblasts were seeded directly onto aligned and random, hydrated collagen scaffolds. While the seeding density was the same for both, the different geometries caused differences in cell density observed after 48 hours. The geometry of the low aspect ratio vessel results in a flat disc-like scaffold, which cells were easily able to settle onto during seeding. In comparison, the aligned collagen scaffolds retained a basic cylindrical geometry. As a result of the curvature, cells were less able to settle on top of the scaffolds, and many cells settled on the bottom of the well plate instead, resulting in an apparent lower cell density on the aligned collagen scaffolds as compared to the random scaffolds prepared in the low-aspect ratio vessel. After 48 hours in culture, those fibroblast cells which did seed to the surface of the aligned collagen scaffolds were oriented and extended along the same axis as the aligned topography (Figure 6B). In contrast, cells on scaffolds prepared in the low aspect ratio vessel, which demonstrated random orientation of micro-features, did not demonstrate any preferential alignment or direction of growth (Figure 6A). An alignment index was generated for each scaffold, where an average value of 1 indicates alignment parallel to the axis of scaffold orientation, an average value of 0 indicates alignment perpendicular to the axis, and an average value of 0.5

indicates random alignment. Cells on aligned scaffolds had an alignment parameter near 1 (0.957 +/- 0.073), which was significantly greater than the alignment parameter for cells on randomly oriented scaffolds (0.445 +/- 0.317; *P*<0.0001) (Figure 6D). Alignment was exponentially distributed on aligned scaffolds, but uniformly distributed on random scaffolds (Figure 6C).

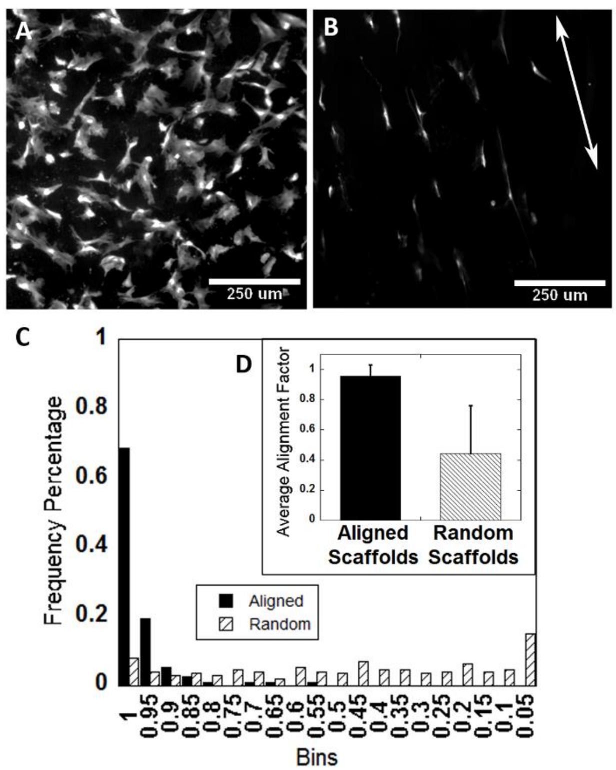

Figure A.6: Alignment of Rat Dermal Fibroblasts on Collagen Scaffolds. (A) GFP-expressing rat dermal fibroblasts cultured on random collagen scaffolds fabricated in low aspect ratio vessels show no preferential alignment; (B) however, GFP expressing rat dermal fibroblasts cultured on aligned collagen scaffolds elongate and orient parallel to the features on the aligned collagen scaffolds (arrow indicates direction of aligned scaffold features). (C and D) Alignment of GFP expressing rat dermal fibroblasts on aligned collagen scaffolds was quantified and the average alignment factor was found to be close to 1 on aligned collagen scaffolds.

Chick DRG explants cultured on aligned collagen scaffolds extended processes along the length of the aligned collagen scaffolds (Figure 7A). DRG explants cultured on randomly oriented collagen scaffolds demonstrated no preferentially oriented outgrowth (Figure 7B).

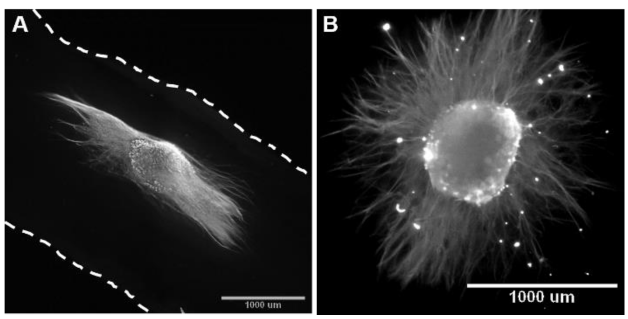

Figure A7: Neurite Outgrowth from DRGs on Collagen Scaffolds: Chick dorsal root ganglia explants were cultured on both aligned and randomly oriented collagen scaffolds and immunolabeled with anti-neurofilament M. (A) Epifluorescence image of DRG extending axons along the length of aligned collagen scaffold (dashed lines indicate the edge of scaffold). (B) Epifluoresence image of DRG explant cultured on a randomly oriented collagen scaffold fabricated in low aspect ratio vessel, which demonstrated no preferentially oriented outgrowth.

A.4 DISCUSSION

We have presented a simple means of generating aligned collagen scaffolds by freezing and sublimation. We hypothesized that constraining the shape of the hydrogels to a vessel with high aspect ratio would induce alignment through anisotropic shrinkage of the gel during lyophilization. We are specifically achieving greater contraction in the radial direction than the axial direction of our cylindrical collagen gels. Although contraction in all three dimensions was not analyzed or quantified as a part of this work, we expect this introduced strain may be transversely isotropic; however, we will refer to this as anisotropic strain (or non-isotropic). The introduction of anisotropic strain to a fibrillar hydrogel induces alignment in the same plane as the tensile strain and/or orthogonal to the direction of compression.[91] Because of the geometry of the cylindrical conduit and extra mass along the length, there is greater resistance to dehydration-induced compaction in the axial direction than the radial direction. This method resulted in collagen scaffolds with highly aligned features on the scaffold surface (Figure 1B and 1C). The formation of these aligned features was dependent on the initial presence of an assembled fibrillar network within the hydrogel and the high aspect ratio vessel.

Collagen sponges have long been fabricated for a variety of medical applications, and a number of commercially available products are currently FDA-approved for human use.[77, 79, 95] Sponges of this type have been traditionally fabricated from a suspension of collagen, rather than a self-assembled, fibrillar hydrogel, which is then frozen and lyophilized to form a porous network that supports cellular infiltration and growth, but generally lacks any preferential alignment. When we fabricated collagen scaffolds from an unassembled collagen suspension in a high-aspect ratio tube, we obtained a porous collagen network that displayed no preferentially aligned topographical features on the surface of scaffolds (Figure 1E). Fibrillar gels that were cast in low aspect ratio vessels also did not have aligned features (Figure 1F). Other groups have modified the approach to prepare collagen sponges to generate scaffolds with aligned pores from collagen suspensions in high aspect ratio conduits. However, the characterization of these scaffolds was largely limited to the interior pore structure and little evidence was presented to characterize the scaffold surface. [86-90] In our approach, the highly aligned surface topography is dependent on the continuous fibrillar hydrogel network prior to freezing and the high aspect ratio conduit used for fabrication. SEM images of cross-sections revealed that the aligned scaffolds fabricated from self-assembled gels cast in cylindrical conduits had a highly porous interior. Instead of appearing as individual, hollow fibers, the topographical features on the scaffold surface may be folds or ridges that arise as the scaffold contracts during lyophilization. It is not yet known if the porous interior is continuous.

Collagen scaffolds demonstrated non-linear strain-stiffening behavior characteristic of collagenous soft tissues (Figure 5).[96-97] Two groups of collagen scaffolds were prepared for mechanical testing. Aligned scaffolds were fabricated in high aspect ratio conduits and displayed preferentially aligned micro-features on the scaffold surface (Figure 1B and 1C). Random scaffolds were fabricated in low aspect ratio vessels and displayed no preferentially aligned micro-features

(Figure 1F). Both groups were made at the same collagen concentration and freezing temperature. Aligned collagen scaffolds displayed a greater elastic modulus, ultimate tensile strength, and strain at ultimate tensile strength than random collagen scaffolds (Table 1). Similar to native tissues and other scaffolds with oriented microstructure, the alignment of collagen features induced stronger and stiffer mechanical behavior.

Several fabrication parameters were easily varied to control features of the scaffold. For example, casting the initial collagen gel in conduits of different diameter allowed control over the final diameter of the aligned scaffold as well as the size of the aligned features of the scaffold. Changing the concentration of the collagen also allowed control of the scaffold diameter, but without changing the size of the individual features. Finally, changing the freezing temperature altered the feature size without changing the scaffold diameter. Freeze-dried collagen scaffolds swell when hydrated, as measured by the increase in scaffold diameter (Figure 2). Swelling occurred in a uniform fashion across all scaffold conditions, preserving the linear trends measured in freeze-dried states. The size of the individual, aligned features was also sensitive to hydration. Thus, these three parameters provide a broad design space for scaffold and feature geometry, which increases the versatility of this simple approach for a variety of applications in tissue engineering.

The freeze-dried scaffold state is preferable for storage and handling, but to seed and support cells, the scaffolds must be presented in a hydrated state. SEM imaging revealed that the aligned topographical features observed in the freeze-dried state were maintained in the hydrated state (Figure 4A). Further examination revealed individual ridges on the surface of aligned features that were on the order of 10µm (Figure 4B). Randomly oriented collagen fibers were visible at 6,500X magnification (Figure 4 C&D). These fibers were approximately 100 nm in diameter and comprised the larger aligned topographical features on the scaffold surface. This interesting result raised the question of which topographical cues would guide cell behavior. Several studies have investigated the influence of feature size on cell alignment. [98-103] Many groups have identified nanoscale features as a critical determinant for guiding cell alignment, which led us to believe that the randomly oriented nanotopography would direct cell alignment in our scaffolds instead of the 10-100µM micro-features.[99-101] We found that both chick DRG explants and rat dermal fibroblasts could sense and respond to the micro-scale aligned topographical cues on the scaffold surface. Individual axons extending from sensory neurons in the DRG explants aligned and extended in the direction of the larger, aligned scaffold features rather than the finer random, nanoscale features (Figure 7A). Individual rat dermal fibroblasts demonstrated similar behavior. We did not attempt to control the orientation of the nanoscale features, nor did we study alternate conditions with aligned nano-features on an otherwise random surface or scaffold. A well-designed study conducted by Moffa et. al. examined the effects of substrates that combined nanofiber topographies with aligned microgrooves on cellular alignment and orientation.[102] They found that substrates with randomly oriented nanofibers and aligned micro groves showed significantly higher cellular alignment and orientation as compared to substrates with random nanofibers and no microgrooves. They examined samples with grooves spaced 15, 50, and 100 µm, distances which compare well with the size of topographical features in our aligned collagen scaffolds. Our results would seem to provide further evidence that aligned micro-features in combination randomly oriented nanofibers are capable of inducing cellular alignment. It is clear from our results that cells and cellular projections sense and respond to the micro-scale alignment, and that this function is not over-ridden by nanoscale features.

This method represents a simple alternative to traditional fabrication of collagen sponges that allows for the introduction of aligned topographical. Previously, generating aligned collagen from collagen gels required complex equipment, whereas our method only requires an incubator, a freezer, and a lyophilizer, which are commonly found in most laboratory settings. Our technique provides another option for preparing aligned collagen scaffolds towards tissue engineered solutions where structural anisotropy is a desirable feature. Skeletal muscle, tendon and ligament, peripheral nerve and spinal cord, and the circumferentially aligned lining of blood vessels have all presented significant challenges to the field of tissue engineering. This simple method holds the potential to serve as a building block for new strategies which address the need presented by replacement of these tissues.

A.5 CONCLUSION

We have developed a rapid and simple method for fabricating collagen scaffolds with highly aligned topographical features, which does not require the need for specialized equipment. This method is dependent on both the high aspect ratio vessels used for fabrication and the fibrillar network within a self-assembled collagen hydrogel. These aligned collagen scaffolds are tunable in both total scaffold diameter and the size of individual, micro-scale topographical. SEM imaging also revealed the presence of a randomly oriented, nanoscale fibrillar topography, consistent with the size of collagen fibrils, that comprises the surface of the larger aligned micro features. The aligned collagen scaffolds supported the growth and alignment of axons from chick DRG explants and rat dermal fibroblasts. Overall, this simple method provides another option to enhance regenerative medicine strategies across a variety of tissue types where tissue anisotropy is critical to functional outcome, such as nerve tissue grafts, engineered tendons and ligaments, or smooth muscle constructs.

BIBLIOGRAPHY

1. Bae, Y. H.; Park, K., Targeted drug delivery to tumors: myths, reality and possibility. *Journal of controlled release : official journal of the Controlled Release Society* **2011,** *153* (3), 198-205.
2. Cheng, Z.; Al Zaki, A.; Hui, J. Z.; Muzykantov, V. R.; Tsourkas, A., Multifunctional nanoparticles: cost versus benefit of adding targeting and imaging capabilities. *Science* **2012,** *338* (6109), 903-10.
3. Banerjee, A.; Pathak, S.; Subramanium, V. D.; G, D.; Murugesan, R.; Verma, R. S., Strategies for targeted drug delivery in treatment of colon cancer: current trends and future perspectives. *Drug discovery today* **2017,** *22* (8), 1224-1232.
4. Kakde, D.; Jain, D.; Shrivastava, V.; Kakde, R.; Patil, A. T., Cancer Therapeutics - Opportunities, Challenges, and Advances in Drug Delivery. *Journal of Applied Pharmaceutical Science* **2011,** *1* (09), 01-10.
5. Toporkiewicz, M.; Meissner, J.; Matusewicz, L.; Czogalla, A.; Sikorski, A. F., Toward a magic or imaginary bullet? Ligands for drug targeting to cancer cells: principles, hopes, and challenges. *International journal of nanomedicine* **2015,** *10*, 1399-414.
6. Kwon, I. K.; Lee, S. C.; Han, B.; Park, K., Analysis on the current status of targeted drug delivery to tumors. *Journal of controlled release : official journal of the Controlled Release Society* **2012,** *164* (2), 108-14.
7. Vasir, J. K.; Labhasetwar, V., Targeted Drug Delivery in Cancer. *Technology in Cancer Research & Treatment* **2005,** *4* (4), 363-374.
8. Horne, M. K.; Nisbet, D. R.; Forsythe, J. S.; Parish, C. L., Three-dimensional nanofibrous scaffolds incorporating immobilized BDNF promote proliferation and differentiation of cortical neural stem cells. *Stem cells and development* **2010,** *19* (6), 843-52.
9. Kuhl, P. R.; Griffith-Cima, L. G., Tethered epidermal growth factor as a paradigm for growth factor-induced stimulation from the solid phase. *Nature Medicine* **1996,** *2* (9), 1022-1027.
10. Ito, Y.; Zheng, J.; Imanishi, Y.; Yonezawa, K.; Kasuga, M., Protein-free cell culture on an artificial substrate with covalently immobilized insulin. *Proceedings of the National Academy of Science* **1996,** *93*, 3598-3601.
11. Ito, Y.; Chen, G.; Imanishi, Y.; Morooka, T.; Nishida, E.; Okabayashi, Y.; Kasuga, M., Differential Control of Cellular Gene Expression by Diffusible and Non-Diffusible EGF. *The Journal of Biochemistry* **2001,** *129*, 733-737.
12. Masand, S. N.; Chen, J.; Perron, I. J.; Hammerling, B. C.; Loers, G.; Schachner, M.; Shreiber, D. I., The effect of glycomimetic functionalized collagen on peripheral nerve repair. *Biomaterials* **2012,** *33* (33), 8353-62.
13. Masand, S. N.; Perron, I. J.; Schachner, M.; Shreiber, D. I., Neural cell type-specific responses to glycomimetic functionalized collagen. *Biomaterials* **2012,** *33* (3), 790-7.

14. Monteiro, G. A.; Fernandes, A. V.; Sundararaghavan, H. G.; Shreiber, D. I., Positively and Negatively Modulating Cell Adhesion to Type-I Collagen Via Peptide Grafting. *Tissue Engineering: Part A* **2011,** *17* (13 and 14), 1663-1673.
15. Sundararaghavan, H. G.; Masand, S. N.; Shreiber, D. I., Microfluidic generation of haptotactic gradients through 3D collagen gels for enhanced neurite growth. *Journal of neurotrauma* **2011,** *28* (11), 2377-87.
16. Sundararaghavan, H. G.; Monteiro, G. A.; Firestein, B. L.; Shreiber, D. I., Neurite growth in 3D collagen gels with gradients of mechanical properties. *Biotechnology and bioengineering* **2009,** *102* (2), 632-43.
17. Prevention, C. f. D. C. a. Rates of TBI-related Emergency Department Visits, Hospitalizations, and Deaths — United States, 2001–2010. http://www.cdc.gov/traumaticbraininjury/data/rates.html.
18. Langlois, J. A.; Rutland-Brown, W.; Wald, M. M., The Epidemiology and Impact of Traumatic Brain Injury: A Brief Overview. *2006* **2006,** *21* (5), 375-378.
19. Ghajar, J., Traumatic brain injury. *The Lancet* **2000,** *356* (9233), 923-929.
20. Maas, A. I. R.; Stocchetti, N.; Bullock, R., Moderate and severe traumatic brain injury in adults. *The Lancet Neurology* **2008,** *7* (8), 728-741.
21. Chao, M. V., Neurotrophins and their receptors: a convergence point for many signalling pathways. *Nature reviews. Neuroscience* **2003,** *4* (4), 299-309.
22. Cardenas-Aguayo, M. C.; Kazim, S. F.; Grundke-Iqbal, I.; Iqbal, K., Neurogenic and Neurotropic Effects of BDNF Peptides in Mouse Hippocampal Primary Neuronal Cell Cultures. *PLOS ONE* **2013,** *8* (1), e53596.
23. Mohtaram, N. K.; Montgomery, A.; Willerth, S. M., Biomaterial-based drug delivery systems for the controlled release of neurotrophic factors. *Biomed Mater* **2013,** *8* (2), 022001.
24. Willerth, S. M.; Sakiyama-Elbert, S. E., Approaches to neural tissue engineering using scaffolds for drug delivery. *Advanced drug delivery reviews* **2007,** *59* (4-5), 325-38.
25. Vutskits, L.; Djebbara-Hannas, Z.; Zhang, H.; Paccaud, J.-P.; Durbec, P.; Rougon, G.; Muller, D.; Kiss, J. Z., 2001 - PSA NCAM modulates BDNF dependent survival and differentiation of cortical neurons. *European Journal of Neuroscience* **2001,** *13*, 1391-1402.
26. Ghosh, A.; Carnahan, J.; Greenberg, M., Requirement for BDNF in Activity-Dependent Survival of Cortical Neurons. *Science* **1994,** *263*, 1618-1623.
27. Galvin, K. A.; Oorschot, D. E., Continuous low-dose treatment with brain-derived neurotrophic factor or neurotrophin-3 protects striatal medium spiny neurons from mild neonatal hypoxia/ischemia: a stereological study. *Neuroscience* **2003,** *118* (4), 1023-1032.
28. Ma, H.; Yu, B.; Kong, L.; Zhang, Y.; Shi, Y., Neural stem cells over-expressing brain-derived neurotrophic factor (BDNF) stimulate synaptic protein expression and promote functional recovery following transplantation in rat model of traumatic brain injury. *Neurochemical research* **2012,** *37* (1), 69-83.
29. Willson, M. L.; McElnea, C.; Mariani, J.; Lohof, A. M.; Sherrard, R. M., BDNF increases homotypic olivocerebellar reinnervation and associated fine motor and cognitive skill. *Brain : a journal of neurology* **2008,** *131* (Pt 4), 1099-112.

30. Zhong, Y.; Bellamkonda, R. V., Biomaterials for the central nervous system. *Journal of the Royal Society, Interface / the Royal Society* **2008,** *5* (26), 957-75.
31. Pettikiriarachchi, J. T. S.; Parish, C. L.; Shoichet, M. S.; Forsythe, J. S.; Nisbet, D. R., Biomaterials for Brain Tissue Engineering. *Australian Journal of Chemistry* **2010,** *63*, 1143-1154.
32. Orive, G.; Anitua, E.; Pedraz, J. L.; Emerich, D. F., Biomaterials for promoting brain protection, repair and regeneration. *Nature reviews. Neuroscience* **2009,** *10* (9), 682-92.
33. Pakulska, M. M.; Ballios, B. G.; Shoichet, M. S., Injectable hydrogels for central nervous system therapy. *Biomed Mater* **2012,** *7* (2), 024101.
34. Cooke, M. J.; Vulic, K.; Shoichet, M. S., Design of biomaterials to enhance stem cell survival when transplanted into the damaged central nervous system. *Soft Matter* **2010,** *6* (20), 4988.
35. Drzewiecki, K. E.; Parmar, A. S.; Gaudet, I. D.; Branch, J. R.; Pike, D. H.; Nanda, V.; Shreiber, D. I., Methacrylation induces rapid, temperature-dependent, reversible self-assembly of type-I collagen. *Langmuir : the ACS journal of surfaces and colloids* **2014,** *30* (37), 11204-11.
36. Gaudet, I. D.; Shreiber, D. I., Characterization of methacrylated type-I collagen as a dynamic, photoactive hydrogel. *Biointerphases* **2012,** *7* (1-4), 25.
37. O'Connell, K. M.; Littleton-Kearney, M. T., The role of free radicals in traumatic brain injury. *Biological research for nursing* **2013,** *15* (3), 253-63.
38. Greve, M. W.; Zink, B. J., Pathophysiology of Traumatic Brain Injury. *Mount Sinai Journal of Medicine* **2009,** *76*, 97-104.
39. Werner, C.; Engelhard, K., Pathophysiology of traumatic brain injury. *British journal of anaesthesia* **2007,** *99* (1), 4-9.
40. Poprac, P.; Jomova, K.; Simunkova, M.; Kollar, V.; Rhodes, C. J.; Valko, M., Targeting Free Radicals in Oxidative Stress-Related Human Diseases. *Trends in pharmacological sciences* **2017,** *38* (7), 592-607.
41. Kehrer, J. P.; Klotz, L. O., Free radicals and related reactive species as mediators of tissue injury and disease: implications for Health. *Critical reviews in toxicology* **2015,** *45* (9), 765-98.
42. Zhang, P. Y.; Xu, X.; Li, X. C., Cardiovascular diseases: oxidative damage and antioxidant protection. *European Review for Medical and Pharmacological Sciences* **2014,** *18*, 3091-3096.
43. Valko, M.; Leibfritz, D.; Moncol, J.; Cronin, M. T.; Mazur, M.; Telser, J., Free radicals and antioxidants in normal physiological functions and human disease. *The international journal of biochemistry & cell biology* **2007,** *39* (1), 44-84.
44. Bryan, N.; Ahswin, H.; Smart, N.; Bayon, Y.; Wohlert, S.; Hunt, J. A., Reactive oxygen species (ROS) – a family of fate deciding molecules pivotal in constructive inflammation and wound healing. *European Cells and Materials* **2012,** *24*, 249-265.
45. Shi, S.; Xue, F., Current Antioxidant Treatments in Organ Transplantation. *Oxidative medicine and cellular longevity* **2016,** *2016*, 8678510.
46. Knight, J. A., Free Radicals, Antioxidants, and the Immune System. *Annals of Clinical & Laboratory Science* **2000,** *30* (2), 145-158.

47. Cowie, J. M. G.; Arrighi, V., *Polymers: Chemistry and Physics of Modern Materials*. 3 ed.; 2007; p 520.
48. Lin, C. C.; Anseth, K. S., PEG hydrogels for the controlled release of biomolecules in regenerative medicine. *Pharmaceutical research* **2009,** *26* (3), 631-43.
49. Sharma, O. P.; Bhat, T. K., DPPH antioxidant assay revisited. *Food Chemistry* **2009,** *113* (4), 1202-1205.
50. Xu, S. Y.; Wu, Y. M.; Ji, Z.; Gao, X. Y.; Pan, S. Y., A modified technique for culturing primary fetal rat cortical neurons. *Journal of biomedicine & biotechnology* **2012,** *2012*, 803930.
51. *Nitric Oxide Protocols*. Humana Press: 1998; Vol. 100.
52. Mironi-Harpaz, I.; Wang, D. Y.; Venkatraman, S.; Seliktar, D., Photopolymerization of cell-encapsulating hydrogels: crosslinking efficiency versus cytotoxicity. *Acta biomaterialia* **2012,** *8* (5), 1838-48.
53. Gormley, A. J.; Chapman, R.; Stevens, M. M., Polymerization amplified detection for nanoparticle-based biosensing. *Nano letters* **2014,** *14* (11), 6368-73.
54. Kobayashi, S.; Uyama, H.; Kimura, S., Enzymatic Polymerization. *Chemical Reviews* **2001,** *101* (12), 3793-3818.
55. Li, M.; Dickinson, C. E.; Finkelstein, E. B.; Neville, C. M.; Sundback, C. A., The role of fibroblasts in self-assembled skeletal muscle. *Tissue engineering. Part A* **2011,** *17* (21-22), 2641-50.
56. Khan, M.; Xu, Y.; Hua, S.; Johnson, J.; Belevych, A.; Janssen, P. M.; Gyorke, S.; Guan, J.; Angelos, M. G., Evaluation of Changes in Morphology and Function of Human Induced Pluripotent Stem Cell Derived Cardiomyocytes (HiPSC-CMs) Cultured on an Aligned-Nanofiber Cardiac Patch. *PloS one* **2015,** *10* (5), e0126338.
57. Liu, Y.; Lu, J.; Li, H.; Wei, J.; Li, X., Engineering blood vessels through micropatterned co-culture of vascular endothelial and smooth muscle cells on bilayered electrospun fibrous mats with pDNA inoculation. *Acta biomaterialia* **2015,** *11*, 114-125.
58. Kobayashi, M.; Lei, N. Y.; Wang, Q.; Wu, B. M.; Dunn, J. C., Orthogonally oriented scaffolds with aligned fibers for engineering intestinal smooth muscle. *Biomaterials* **2015,** *61*, 75-84.
59. Li, X.; Snedeker, J. G., Wired silk architectures provide a biomimetic ACL tissue engineering scaffold. *Journal of the mechanical behavior of biomedical materials* **2013,** *22*, 30-40.
60. Cai, C.; Chen, C.; Chen, G.; Wang, F.; Guo, L.; Yin, L.; Feng, D.; Yang, L., Type I collagen and polyvinyl alcohol blend fiber scaffold for anterior cruciate ligament reconstruction. *Biomed Mater* **2013,** *8* (3), 035001.
61. Beason, D. P.; Connizzo, B. K.; Dourte, L. M.; Mauck, R. L.; Soslowsky, L. J.; Steinberg, D. R.; Bernstein, J., Fiber-aligned polymer scaffolds for rotator cuff repair in a rat model. *Journal of shoulder and elbow surgery / American Shoulder and Elbow Surgeons ... [et al.]* **2012,** *21* (2), 245-50.
62. Breidenbach, A. P.; Gilday, S. D.; Lalley, A. L.; Dyment, N. A.; Gooch, C.; Shearn, J. T.; Butler, D. L., Functional tissue engineering of tendon: Establishing

biological success criteria for improving tendon repair. *Journal of biomechanics* **2014,** *47* (9), 1941-8.
63. Nikkhah, M.; Eshak, N.; Zorlutuna, P.; Annabi, N.; Castello, M.; Kim, K.; Dolatshahi-Pirouz, A.; Edalat, F.; Bae, H.; Yang, Y.; Khademhosseini, A., Directed endothelial cell morphogenesis in micropatterned gelatin methacrylate hydrogels. *Biomaterials* **2012,** *33* (35), 9009-18.
64. Cornwell, K. G.; Pins, G. D., Enhanced proliferation and migration of fibroblasts on the surface of fibroblast growth factor-2-loaded fibrin microthreads. *Tissue engineering. Part A* **2010,** *16* (12), 3669-77.
65. Martens, W.; Sanen, K.; Georgiou, M.; Struys, T.; Bronckaers, A.; Ameloot, M.; Phillips, J.; Lambrichts, I., Human dental pulp stem cells can differentiate into Schwann cells and promote and guide neurite outgrowth in an aligned tissue-engineered collagen construct in vitro. *FASEB journal : official publication of the Federation of American Societies for Experimental Biology* **2014,** *28* (4), 1634-43.
66. Georgiou, M.; Bunting, S. C.; Davies, H. A.; Loughlin, A. J.; Golding, J. P.; Phillips, J. B., Engineered neural tissue for peripheral nerve repair. *Biomaterials* **2013,** *34* (30), 7335-43.
67. Bettinger, C. J.; Langer, R.; Borenstein, J. T., Engineering substrate topography at the micro- and nanoscale to control cell function. *Angew Chem Int Ed Engl* **2009,** *48* (30), 5406-15.
68. Dahlin, R. L.; Kasper, F. K.; Mikos, A. G., Polymeric nanofibers in tissue engineering. *Tissue engineering. Part B, Reviews* **2011,** *17* (5), 349-64.
69. Li, M.; Mondrinos, M. J.; Gandhi, M. R.; Ko, F. K.; Weiss, A. S.; Lelkes, P. I., Electrospun protein fibers as matrices for tissue engineering. *Biomaterials* **2005,** *26* (30), 5999-6008.
70. Ma, Z.; Kotaki, M.; Inai, R.; Ramakrishna, S., Potential of Nanofiber Matrix as Tissue-Engineering Scaffolds. *Tissue engineering. Part A* **2005,** *11* (1/2), 101-109.
71. Wang, Y.; Yao, M.; Zhou, J.; Zheng, W.; Zhou, C.; Dong, D.; Liu, Y.; Teng, Z.; Jiang, Y.; Wei, G.; Cui, X., The promotion of neural progenitor cells proliferation by aligned and randomly oriented collagen nanofibers through beta1 integrin/MAPK signaling pathway. *Biomaterials* **2011,** *32* (28), 6737-44.
72. Ricard-Blum, S., The collagen family. *Cold Spring Harbor perspectives in biology* **2011,** *3* (1), a004978.
73. Antoine, E. E.; Vlachos, P. P.; Rylander, M. N., Review of collagen I hydrogels for bioengineered tissue microenvironments: characterization of mechanics, structure, and transport. *Tissue engineering. Part B, Reviews* **2014,** *20* (6), 683-96.
74. Sell, S. A.; McClure, M. J.; Garg, K.; Wolfe, P. S.; Bowlin, G. L., Electrospinning of collagen/biopolymers for regenerative medicine and cardiovascular tissue engineering. *Advanced drug delivery reviews* **2009,** *61* (12), 1007-19.
75. Kolacna, L.; Bakesova, J.; Varga, F.; Kostakova, E.; Planka, L.; Necas, A.; Lukas, D.; Amler, E.; Pelouch, V., Biochemical and Biophysical Aspects of Collagen Nanostructure in the Extracellular Matrix. *Physiology Research* **2007,** *56* (S1), S51-S60.

76. Cheung, H.-Y.; Lau, K.-T.; Lu, T.-P.; Hui, D., A critical review on polymer-based bio-engineered materials for scaffold development. *Composites Part B: Engineering* **2007,** *38* (3), 291-300.
77. Glowacki, J.; Mizuno, S., Collagen scaffolds for tissue engineering. *Biopolymers* **2008,** *89* (5), 338-44.
78. Zhu, J.; Marchant, R. E., Design properties of hydrogel tissue-engineering scaffolds. *Expert review of medical devices* **2011,** *8* (5), 607-26.
79. Abou Neel, E. A.; Bozec, L.; Knowles, J. C.; Syed, O.; Mudera, V.; Day, R.; Hyun, J. K., Collagen--emerging collagen based therapies hit the patient. *Adv Drug Deliv Rev* **2013,** *65* (4), 429-56.
80. Lee, C.; Singla, A.; Lee, Y., Biomedical applications of collagen. *International Journal of Pharmaceutics* **2001,** *221*, 1-22.
81. Dong, B.; Arnoult, O.; Smith, M. E.; Wnek, G. E., Electrospinning of collagen nanofiber scaffolds from benign solvents. *Macromolecular rapid communications* **2009,** *30* (7), 539-42.
82. Cheng, X.; Gurkan, U. A.; Dehen, C. J.; Tate, M. P.; Hillhouse, H. W.; Simpson, G. J.; Akkus, O., An electrochemical fabrication process for the assembly of anisotropically oriented collagen bundles. *Biomaterials* **2008,** *29* (22), 3278-88.
83. Girton, T. S.; Dubey, N.; Tranquillo, R. T., Magnetic-Induced Alignment of Collagen Fibrils in Tissue Equivalents. *Methods in Molecular Medicine* **1999,** *18*, 67-73.
84. Wray, L. S.; Rnjak-Kovacina, J.; Mandal, B. B.; Schmidt, D. F.; Gil, E. S.; Kaplan, D. L., A silk-based scaffold platform with tunable architecture for engineering critically-sized tissue constructs. *Biomaterials* **2012,** *33* (36), 9214-24.
85. Stoppel, W. L.; Hu, D.; Domian, I. J.; Kaplan, D. L.; Black, L. D., 3rd, Anisotropic silk biomaterials containing cardiac extracellular matrix for cardiac tissue engineering. *Biomed Mater* **2015,** *10* (3), 034105.
86. Chamberlain, L. J.; Yannas, I. V.; Arrizabalaga, A.; Hsu, H.-P.; Norregaard, T. V.; Spector, M., Early peripheral nerve healing in collagen and silicone tube implants: Myofibroblasts and the cellular response. *Biomaterials* **1998,** *19*, 1393-1403.
87. Chamberlain, L. J.; Yannas, I. V.; Hsu, H.-P.; Strichartz, G.; Spector, M., Collagen-GAG Substrate Enhances the Quality of Nerve Regeneration through Collagen Tubes up to Level of Autograft. *Experimental neurology* **1998,** *154*, 315-329.
88. Chamberlain, L. J.; Yannas, I. V.; Hsu, H.-P.; Spector, M., Connective Tissue Response to Tubular Implants for Peripheral Nerve Regeneration: The Role of Myofibroblasts. *The Journal of Comparitive Neurology* **2000,** *417*, 415-430.
89. Chamberlain, L. J.; Yannas, I. V.; Hsu, H.-P.; Strichartz, G.; Spector, M., Near-Terminus Axonal Structure and Function Following Rat Sciatic Nerve Regeneration Through a Collagen-GAG Matrix in a Ten-Millimeter Gap. *Journal of Neuroscience Research* **2000,** *60*, 666-677.
90. Madaghiele, M.; Sannino, A.; Yannas, I. V.; Spector, M., Collagen-based matrices with axially oriented pores. *Journal of biomedical materials research. Part A* **2008,** *85* (3), 757-67.

91. Vader, D.; Kabla, A.; Weitz, D.; Mahadevan, L., Strain-Induced Alignement in Collagen Gels. *PloS one* **2009,** *4* (6), e5902.
92. Girton, T. S.; Barocas, V. H.; Tranquillo, R. T., Confined Compression of a Tissue-Equivalent: Collagen Fibril and Cell Alignment in Response to Anisotropic Strain. *Journal of Biomechanical Engineering* **2002,** *124* (5), 568.
93. Knapp, D. M.; Helou, E. F.; Tranquillo, R. T., A Fibrin or Collagen Gel Assay for Tissue Cell Chemotaxis: Assesment of Fibroblast Chemotaxis to GRGDSP. *Experimental Cell Research* **1999,** *243*.
94. Bray, D. F.; Bagu, J.; Koegler, P., Comparison of hexamethyldisilazane (HDMS), Peldri II, and critical-point drying methods for scanning electron microscopy of biological specimins. *Microscopy Research and Technique* **1993,** *26* (6), 489-495.
95. Mohd Hilmi, A. B.; Halim, A. S., Vital roles of stem cells and biomaterials in skin tissue engineering. *World journal of stem cells* **2015,** *7* (2), 428-36.
96. Storm, C.; Pastore, J. J.; MacKintosh, F. C.; Lubensky, T. C.; Janmey, P. A., Nonlinear elasticity in biological gels. *Nature* **2005,** *435*, 191-194.
97. Y.C., F., *A First Course In Continuum Mechanics*. 2 ed.; Prentice-Hall, Inc.: Englewood Cliffs, NJ, 1977; p 340.
98. Fozdar, D. Y.; Lee, J. Y.; Schmidt, C. E.; Chen, S., Selective axonal growth of embryonic hippocampal neurons according to topographic features of various sizes and shapes. *International journal of nanomedicine* **2011,** *6*, 45-57.
99. Jana, S.; Leung, M.; Chang, J.; Zhang, M., Effect of nano- and micro-scale topological features on alignment of muscle cells and commitment of myogenic differentiation. *Biofabrication* **2014,** *6* (3), 035012.
100. Li, J. Y.; Ho, Y. C.; Chung, Y. C.; Lin, F. C.; Liao, W. L.; Tsai, W. B., Preparation of micron/submicron hybrid patterns via a two-stage UV-imprint technique and their dimensional effects on cell adhesion and alignment. *Biofabrication* **2013,** *5* (3), 035003.
101. Loesberg, W. A.; te Riet, J.; van Delft, F. C.; Schon, P.; Figdor, C. G.; Speller, S.; van Loon, J. J.; Walboomers, X. F.; Jansen, J. A., The threshold at which substrate nanogroove dimensions may influence fibroblast alignment and adhesion. *Biomaterials* **2007,** *28* (27), 3944-51.
102. Moffa, M.; Sciancalepore, A. G.; Passione, L. G.; Pisignano, D., Combined nano- and micro-scale topographic cues for engineered vascular constructs by electrospinning and imprinted micro-patterns. *Small* **2014,** *10* (12), 2439-50.
103. Seunarine, K.; Curtis, A. S. G.; Meredith, D. O.; Wilkinson, C. D. W.; Riehle, M. O.; Gadegaard, N., A Hierarchical Response of Cells to Perpendicular Micro- and Nanometric Textural Cues. *IEEE Transactions on Nanobioscience* **2009,** *8* (3), 219-225.